Lawrence Berkeley National Laboratory
Recent Work

Title

MODELING AND OPTIMIZATION OF LI-ALLOY/METAL-SULFIDE MOLTEN SALT BATTERIES M.S.Thesis

Permalink

https://escholarship.org/uc/item/06n9v90q

Author

Mason, A.A.

Publication Date

1988-09-01

eScholarship.org Powered by the California Digital Library
University of California

LBL-26159 c2

Lawrence Berkeley Laboratory

UNIVERSITY OF CALIFORNIA

RECEIVED
LAWRENCE
BERKELEY LABORATORY

JUL 24 1989

LIBRARY AND
DOCUMENTS SECTION

Materials & Chemical Sciences Division

Modeling and Optimization of Li-Alloy/Metal-Sulfide Molten Salt Batteries

A.A. Mason
(M.S. Thesis)

September 1988

TWO-WEEK LOAN COPY

This is a Library Circulating Copy
which may be borrowed for two weeks.

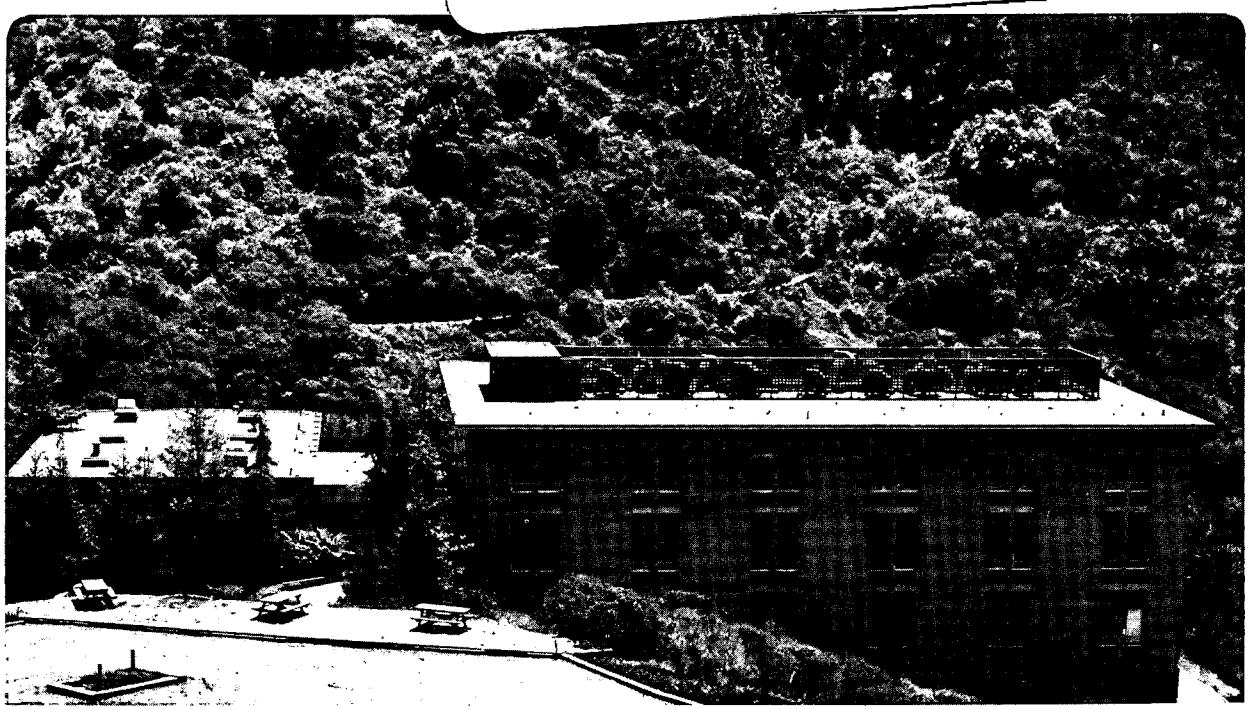

Prepared for the U.S. Department of Energy under Contract Number DE-AC03-76SF00098.

LBL-26159 c2

DISCLAIMER

This document was prepared as an account of work sponsored by the United States Government. While this document is believed to contain correct information, neither the United States Government nor any agency thereof, nor the Regents of the University of California, nor any of their employees, makes any warranty, express or implied, or assumes any legal responsibility for the accuracy, completeness, or usefulness of any information, apparatus, product, or process disclosed, or represents that its use would not infringe privately owned rights. Reference herein to any specific commercial product, process, or service by its trade name, trademark, manufacturer, or otherwise, does not necessarily constitute or imply its endorsement, recommendation, or favoring by the United States Government or any agency thereof, or the Regents of the University of California. The views and opinions of authors expressed herein do not necessarily state or reflect those of the United States Government or any agency thereof or the Regents of the University of California.

LBL-26159

Modeling and Optimization of Li-Alloy/Metal-Sulfide Molten Salt Batteries

Andrew A. Mason

Department of Chemical Engineering
University of California

and

Materials and Chemical Sciences Division
Lawrence Berkeley Laboratory
1 Cyclotron Road
Berkeley, CA 94720

September 28, 1988

This work was supported by the Assistant Secretary of Conservation and Renewable Energy, Office of Energy Storage and Distribution, Energy Storage Division of the U.S. Department of Energy under Contract No. DE-AC03-76SF00098

Modeling and Optimization of Li-Alloy/Metal-Sulfide Molten-Salt Batteries

by

Andrew Alan Mason

Abstract

A computer model for the LiAl/FeS_x molten-salt battery system (prismatic geometry), which uses input data from experimental test cells, is presented. Optimizations of the negative-to-positive capacity ratio and the number of electrodes per cell are considered. The LiAl/FeS, LiAl/FeS_2 (two-plateau operation), and LiAl/FeS_2 (upper-plateau operation) battery systems are compared. (Upper-plateau operation refers to the discharge of FeS_2 to Li_2FeS_2, and two-plateau operation refers to complete discharge to Fe and Li_2S.) While the specific energies are similar for all three systems, the specific power near the end of discharge is highest for the upper-plateau FeS_2 system.

A similar model for a multi-electrode LiAl/FeS_2 cylindrical cell (upper-plateau operation) is also presented. A simplified version of this model, which does not account for the bus and post resistances, is used to show that the experimental data currently available in the literature are not appropriate for use with this model. In spite of this disappointing conclusion, the effects of the positive current collector radius, the cell height, and the number of positive electrodes on specific energy and specific power are examined.

Acknowledgements

I would like to thank Professor John Newman for all he has taught me. I hope his problem solving methodology will be reflected in my future endeavors. I would also like to thank my committee members, Thomas Devine and Elton Cairns, for their valuable comments. Finally, I would like to thank the members of my research group for their help and friendship.

This work was supported by the Assistant Secretary for Conservation and Renewable Energy, Office of Energy Storage and Distribution of the U. S. Department of Energy under Contract DE-AC03-76SF00098.

Contents

CHAPTER 1

Introduction

The purpose of this introduction is threefold. First, the history of LiAl/FeS_x battery development is discussed. Second, a review of the literature is presented. Finally, an overview of the thesis is given.

The development of LiAl/FeS and LiAl/FeS_2 secondary, molten-salt batteries is desirable because they offer the prospect of high specific energy and high specific power. Possible applications of these batteries include electric vehicle propulsion and load leveling. Extensive research and development has been directed towards Li(Alloy)/FeS_x batteries following their conception in 1973 [1]. Bernardi [2] has reviewed thermodynamic, kinetic, and physical data for the LiAl, FeS, and FeS_2 electrodes. The electrode reactions are given in Appendix C. A summary of a large development program for the LiAl/FeS cell at Argonne National Laboratory (ANL) has been presented by Gay *et al.* [1]. Kaun *et al.* [3] have discussed recent advances in LiAl/FeS and LiAl/FeS_2 battery development. A shematic of one possible cell design is presented in Figure 10 of Chapter 3.

The LiAl/FeS and LiAl/FeS_2 systems were an outgrowth of an attempt to design a battery based on the highly energetic Li/S couple [1]. Problems associated with the Li/S battery included volatility and solubility of active materials, corrosion of cell components, and

the need to contain the liquid lithium electrode. In order to help alleviate these problems, the α-β LiAl alloy negative and FeS positive electrodes were developed. The FeS_2 electrode, which was developed later, provides a higher voltage alternative to the FeS electrode but suffers from corrosion problems due to increased sulfur activity [2]. All of these electrodes are solids at normal operating temperatures (375-500°C). The only material that has been found to be suitable for the current collector of the FeS_2 electrode is molybdenum; researchers have been searching for other alternatives [4] [5]. Low-carbon steel is well suited for use as the current collector material for the negative electrode [5]. Electrodes with alternate alloy compositions or electrodes that contain additives, or both, has been a continuing subject of research for the positive electrode [6], [7] and the negative electrode [8].

The first sealed engineering lithium metal sulfide cells built by ANL used a cylindrical design with a central positive electrode. In order to improve volumetric energy density, development efforts were redirected towards vertically oriented, prismatic cells because they can be stacked more compactly in a battery case [5]. Recently, a new cylindrical cell design with multiple positive electrodes has been proposed [9], in which a simple rod through the center of the positive electrode acts as the current collector. This design minimizes the expenses associated with the requirement that the current collector be fabricated from molybdenum.

Molten salts of various compositions have been used as electrolytes in these systems. Most of the development work on the FeS electrode has been concentrated on its behavior in LiCl-KCl electrolyte at temperatures between 400 and 500°C [2]. The eutectic composition of this mixture is 58 mol% LiCl (m.p. 352°C) [8]. In addition to non-eutectic compositions of this mixture, ternary mixtures have been studied for use with both FeS and FeS_2 cells [1], [8]. For example, Kaun [7] successfully used 25 mol% LiCl, 37 mol% LiBr, 38 mol% KBr (m.p. 310°C) for a LiAl/FeS_2 cell. The liquidus of Kaun's electrolyte extends over a Li^+/K^+ range of 1.25 to 2.6 as opposed to a range of 1.25 to 1.81 for LiCl-KCl. The broader liquidus tends to avoid salt crystallization [7]. In addition, the FeS_2 reaction rate is faster in LiCl-LiBr-KBr than LiCl-KCl [3].

Separators for these cells are usually constructed of magnesium oxide (MgO) or boron nitride (BN). Researchers continue to explore options for separator materials and wetting procedures.

The work presented here is an extension of work done by Trost on the prismatic LiAl/FeS cell [10], [11]. Trost has presented a computer program, which is a predecessor to the one developed for this work, with which he has shown how to optimize the design specifications for several cell components: the current collector grid weight, the current collector grid area, and the interconnecting bus and post weights. This optimization consists of determining the design specifications such that a desired combination of specific energy and specific power is achieved.

Tiedemann and Newman presented a battery model that described the transient behavior of a lead-acid cell [12] and a current collector grid model that showed the competing effects of electrochemical and electronic voltage losses [13].

Gu *et al.* [14] have combined simple experiments with mathematical models to identify important voltage losses in batteries with prismatic geometries. They have been able to apply this approach to improve battery power density.

Asai *et al.* [15] optimized current collector designs for tall tubular lead/acid cells using an analysis of the reaction distributions within the cell.

The objective of this work is to use computer models of LiAl/FeS_x molten-salt battery systems, which use input data from experimental test cells, to show how these systems can be designed for optimum specific energy and specific power.

Chapter two presents the data from the literature that were used to predict the electrochemical behavior of the LiAl/FeS_x cells. The modeling and optimization work that was done for the prismatic cell geometry is presented in Chapter three. It is shown how one can optimize the number of electrodes in a battery and the negative-to-positive capacity ratio. In addition three different battery systems with equal capacities are compared by first choosing a particular battery design and then optimizing this design for maximum specific energy in each system. A mathematical model that can be used to predict the energy and power characteristics of multi-rod, cylindrical

cells is presented in Chapter three. A simplified version of this model is used to estimate the effects of the positive current collector radius, the cell height, and the number of positive electrodes on specific energy and specific power. Chapter five contains a partial review of the literature pertaining to electronic conductivities in porous electrodes. The purpose of this final chapter is to give some future researcher a starting point for doing work in this area.

CHAPTER 2

Input Data and Curve Fitting

2.1. Introduction

Experimental data from small, prismatic test cells were used to characterize the electrochemical behavior of the cells. A drawing of one of these test cells is presented in Figure 1. The test cells were constructed with heavy current collectors and terminals so that the current densities across the electrode faces would be uniform and the voltage losses due to cell hardware would be negligible.

Apparent open-circuit potentials and area-specific-resistance values for each electrode were collected as a function of depth of discharge (*DOD*). The apparent open-circuit potential of the cell (U_{cell}) is the voltage difference between the terminals of the cell measured at a given length of time after a current interruption. The length of time after current interruption was 15 seconds for all the data used in this work. A reference electrode placed at the half thickness of the separator was used to divide the apparent open-circuit potential of the cell into values associated with the positive and negative electrodes. Thus,

$$U_{cell} = U_{+} - U_{-} \ . \qquad (2\text{-}1)$$

The area-specific resistance of the cell is defined by,

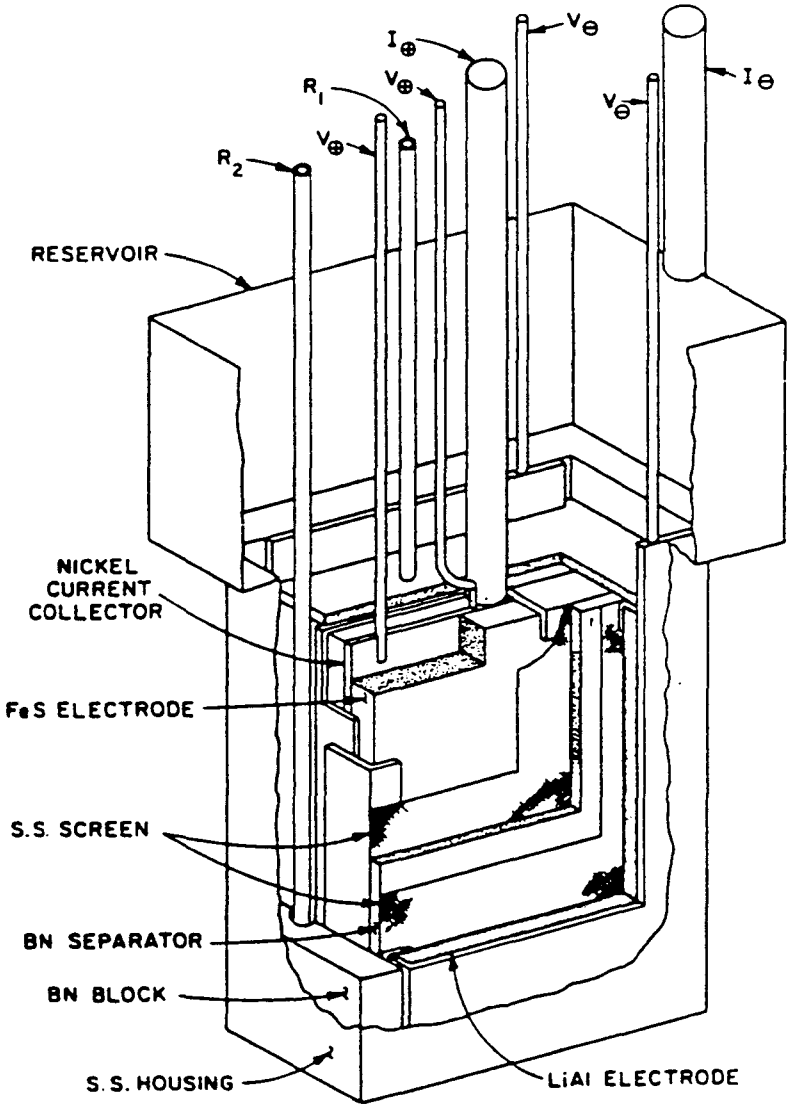

Figure 1. Experimental test bi-cell for FeS data.

Reproduced from reference 17, p. 69. Heavy current collectors are used to promote uniform current distributions across the faces of the positive and two negative half electrodes.

$$ASR_{cell} = \frac{U_{cell} - V_{cell}}{i} , \qquad (2\text{-}2)$$

where ASR_{cell} is in $\Omega \cdot cm^2$, V_{cell} is the closed-circuit potential of the cell (volts), and i is the current density (A/cm^2). The current density and ASR values are based on separator area. The ASR_{cell} is sometimes called the apparent electrochemical impedance by some researchers [16]. Using the reference electrode, the ASR values were split into values associated with each electrode. The area-specific resistance is a strong function of depth of discharge and current interruption time; however, it is almost independent of current density for the lower current range (0 to 200 mA/cm^2) [16], [5]. A brief discussion of reference electrodes and the current interruption technique is given in Appendix F.

The experimental values were fitted with curves whose equations appear in subroutines of the program. In the following discussion the electrode potentials are given versus an α-β LiAl reference electrode. The data are plotted as a function of depth of discharge (*DOD*), which is the fraction of available capacity that has been used. Each of the ASR values includes one-half of the separator resistance.

2.2. Discussion of Curves

2.2.1. LiAl Electrode

The data used for the LiAl electrode were collected from a LiAl/FeS test bicell by S. Higuchi, F. J. Martino, A. S. Claveria, and W. E. Moore [17]. The electrolyte was 54 wt.% LiCl, 46 wt.% KCl, and the cell was operated at 460°C. Figures 2 and 3 give the curve

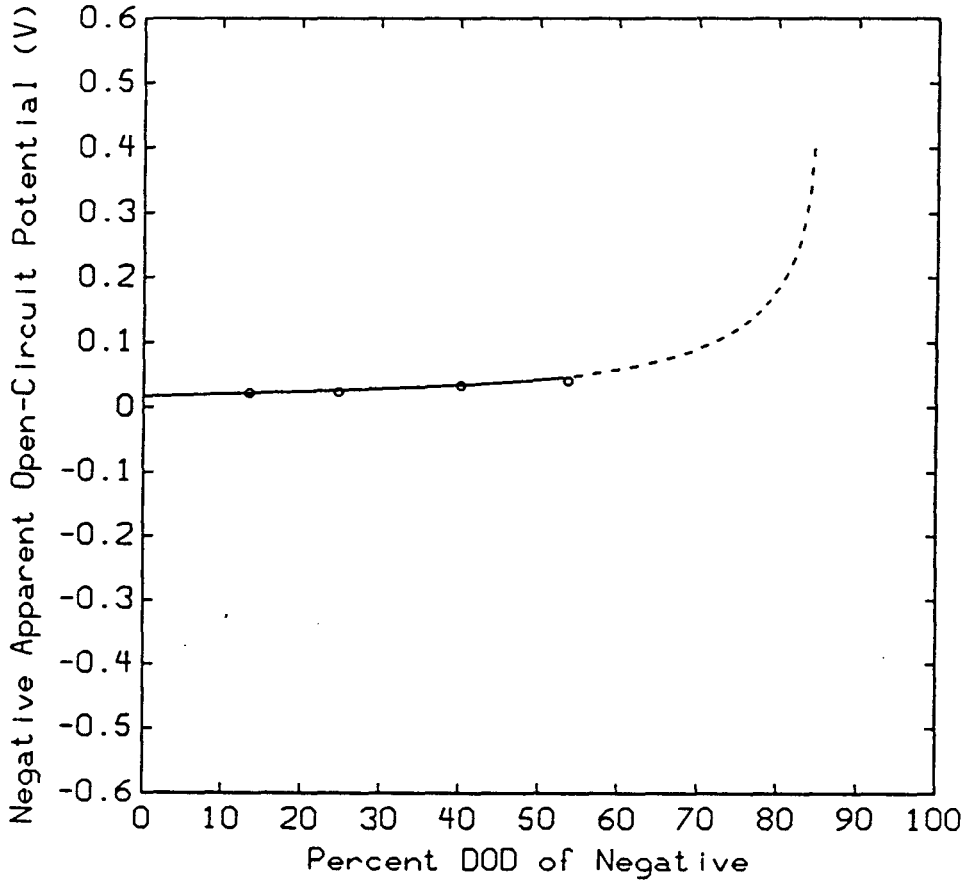

Figure 2. LiAl Electrode Potentials. The solid line is the curve fit. The dashed line represents an extrapolation beyond experimental data (reference 17, p. 71).

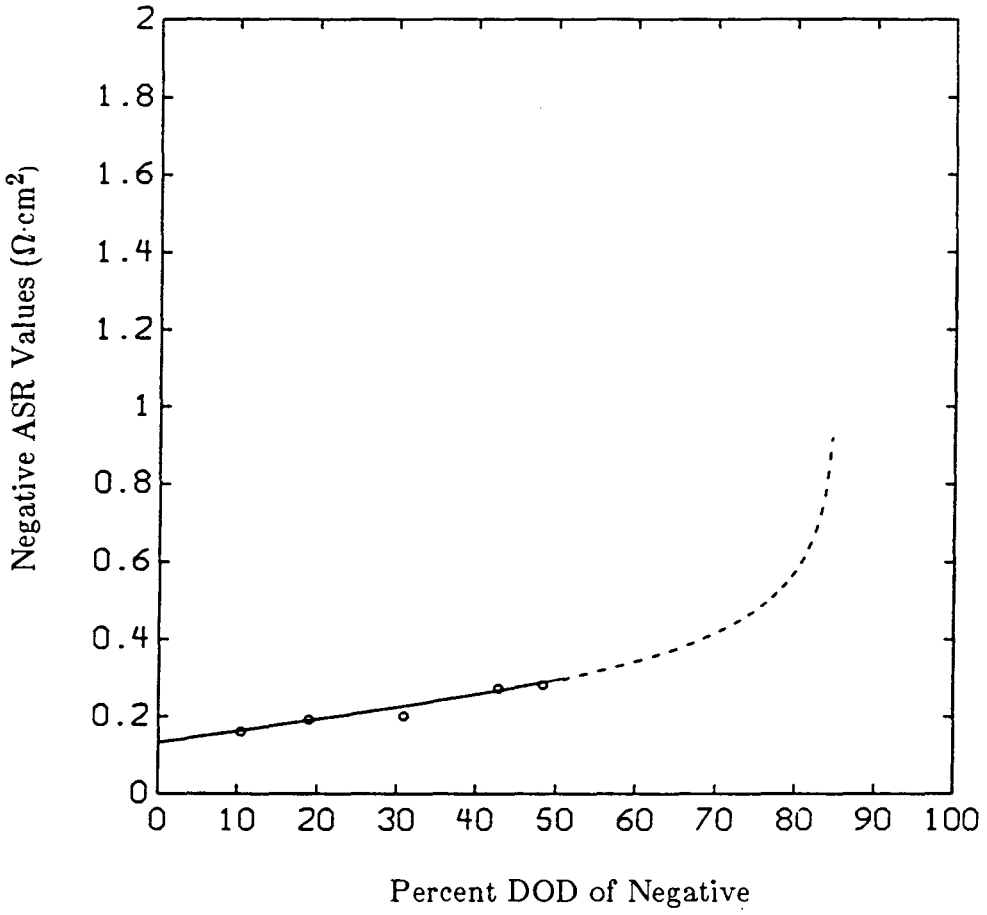

Figure 3. LiAl Area-Specific-Resistance Values. The solid line is the curve fit. The dashed line represents an extrapolation beyond experimental data (reference 17, p. 71).

fits of the data; at full charge (0% DOD) the alloy contained 50 atomic percent Li, and it would have become pure Al if it had been fully discharged. The dotted lines show how the data were extrapolated. The data were extrapolated in this manner so that the cell voltage would drop dramatically at 85% DOD, which is considered to be complete utilization of the available Li because the α phase of the LiAl alloy extends to about 7 to 10 percent Li [18]. In the past, researchers have plotted U_- and ASR_- values as a function of utilization of the positive capacity (the capacity-limiting electrode in the cell). The data have been plotted versus utilization of negative capacity in these Figures in order to facilitate comparison of various experiments.

2.2.2. FeS Electrode

The data for the FeS electrode were obtained from the same LiAl/FeS prismatic bicell as the data that were used for the LiAl electrode. The curve fits were described by Newman *et al.* [17], and they are shown in Figures 4 and 5.

2.2.3. Two-Plateau FeS_2 Electrode

The dashed line in Figure 6 gives the theoretical-open-circuit potential of the FeS_2 electrode as a function of depth of discharge [2]. The segment of the curve from 50% DOD (Li_2FeS_2) to 100% DOD (pure Fe and Li_2S) is called the lower plateau; the rest of the curve is the upper plateau. The data shown in Figures 6 and 7 come from cells that where designed to operate on both the upper and lower pla-

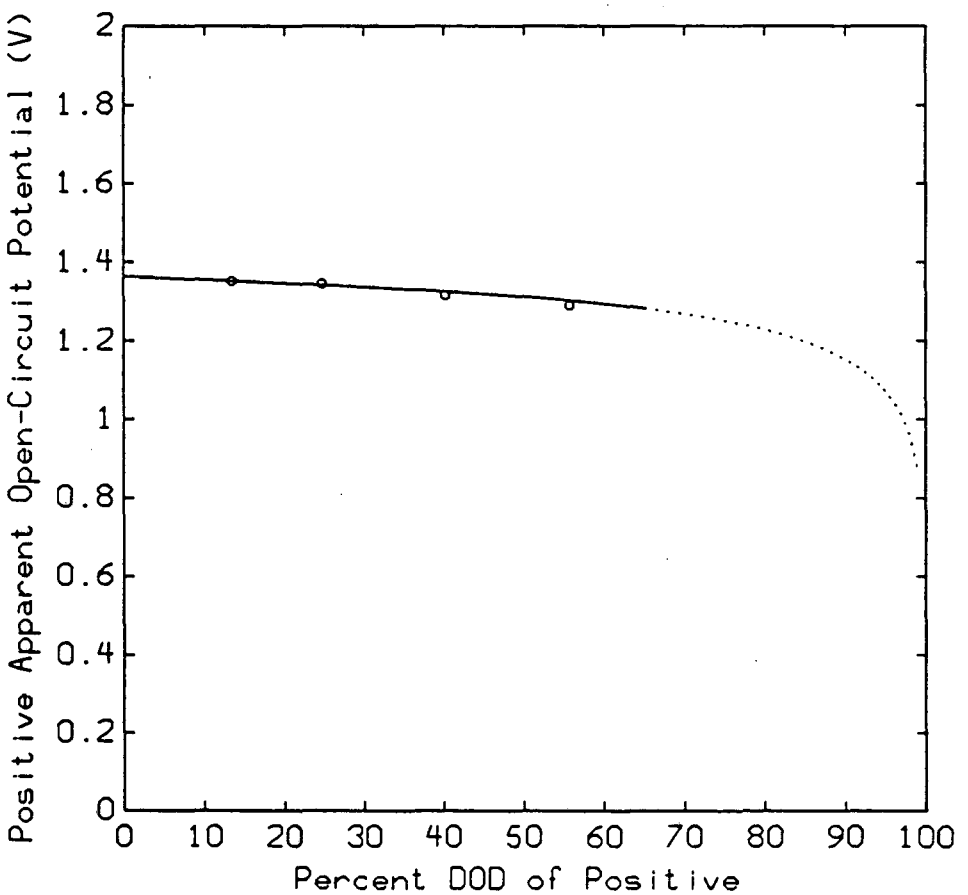

Figure 4. FeS Electrode Potentials. The solid line is the curve fit. The dashed line represents an extrapolation beyond experimental data (reference 17, p. 71)

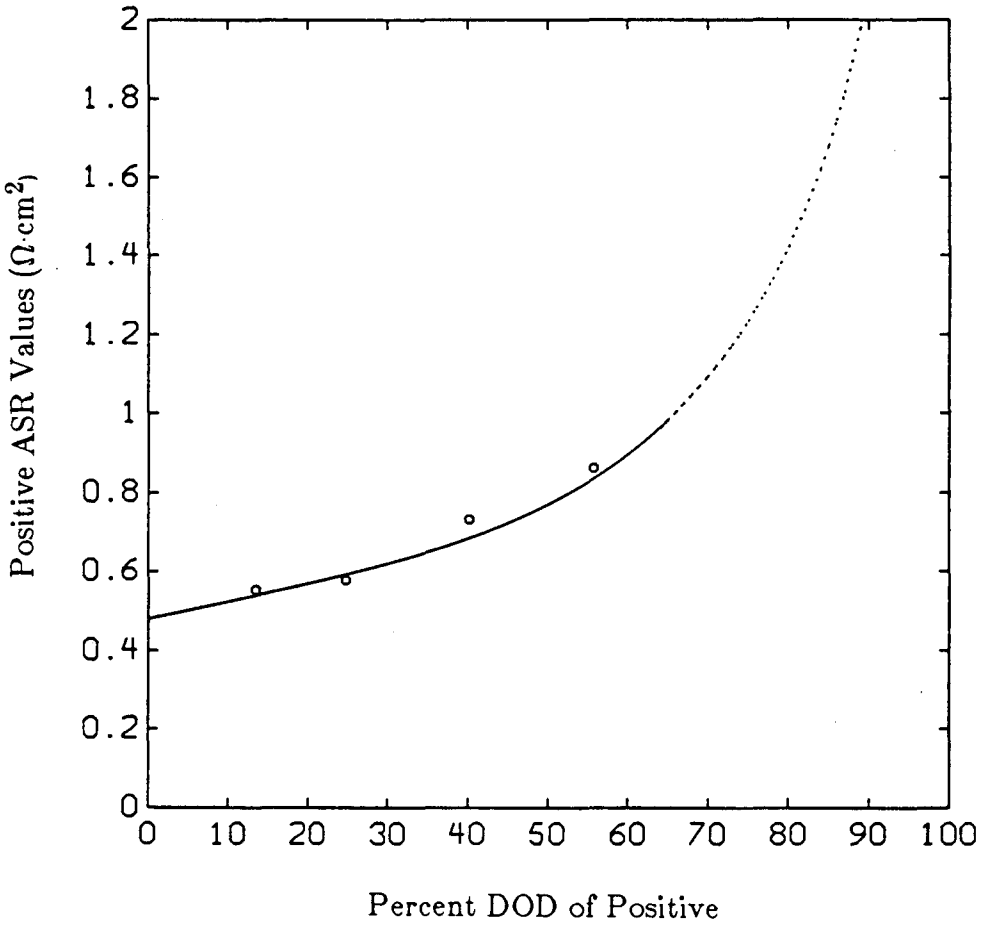

Figure 5. FeS Area-Specific-Resistance Values. The solid line is the curve fit. The dashed line represents an extrapolation beyond experimental data (reference 17, p. 71)

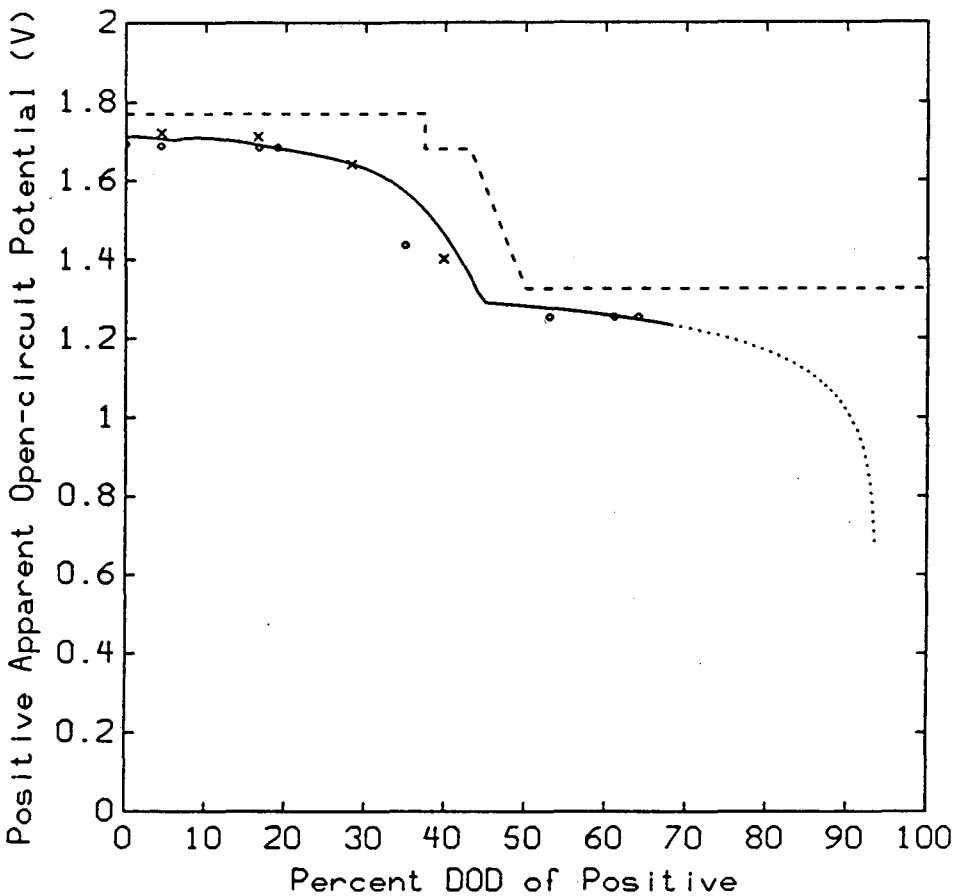

Figure 6. Two-plateau FeS_2 Potentials. The solid line is the curve fit. The dashed line shows the thermodynamic open-circuit potential at 450°C (reference 2, p. 103). The dotted line represents an extrapolation beyond experimental data.

o's from reference 19, p. 17; i=37 mA/cm^2

x's from reference 19, p. 17; i=74 mA/cm^2

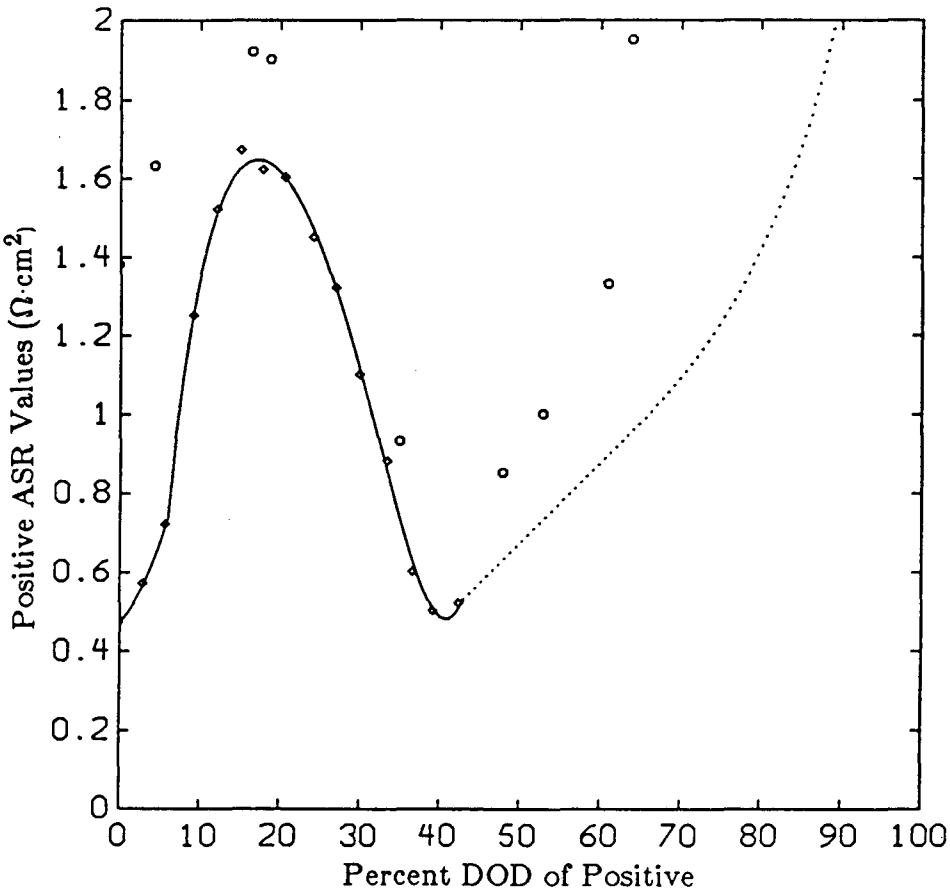

Figure 7. Area-Specific-Resistance of Two-plateau FeS_2. The solid line is curve fit of data from reference 16, p. 13 (diamonds). The dotted line shows how the data are extrapolated. The circles represent data from reference 19, p. 17 (i=37 mA/cm^2).

teaus (called two-plateau or 2-P operation). The data in Figure 6 and the data represented by circles in Figure 7 were collected from a sealed, compact, prismatic monocell [19]. The electrolyte in this monocell was probably 54 wt.% LiCl and 46 wt.% KCl. It can be seen from Figure 6 that there are definite differences between sets of experimental data. These differences, coupled with the extrapolations given in Figures 2 and 3 cause uncertainties in predicting the electrochemical behavior of the cells. These uncertainties, which cast doubt upon the exact energy and power values obtained from the model, do not affect the conclusions of this work. The data reached the lower plateau at a value of DOD that was less than 50%. This could be attributed to material in the electrode bed reacting at different rates, to some parts of the electrode not reacting at all, or to another cause of capacity loss. The curve was extrapolated (dotted line) using the curve fit for the FeS electrode (since $Li_2FeS_2 \approx Li_2S + FeS$) shifted by 5% DOD. This extrapolation is prone to error because the FeS data were taken from a different experiment with, among other things, different positive loading density and different electrolyte.

The diamonds in Figure 7 correspond to data published by Redey *et al.* [16]. The electrolyte was LiCl-KCl at its eutectic composition, and the cell was operated at 450°C. This set of data was chosen for the ASR curve fit because it comes from more recent experiments. The differences between the sets of data do not have a large impact on the modeled cell behavior because the current densities in the cell are

small ($i \approx 100$ mA/cm^2). Once again the data were extrapolated using the FeS curve fit.

Redey *et al.* [16] gave closed-circuit voltage curves instead of U curves. Figures 6 and 7 were combined to calculate the closed-circuit voltage using Equation (2-2). The resulting curve matched the curve in Figure 1 of reference [16].

2.2.4. Upper-Plateau FeS_2 Electrode

Figure 8 shows the curve fit of ASR data collected from Kaun's upper-plateau (U-P) LiAl/FeS_2 cell [20]. The major difference between the FeS_2 electrode used in Kaun's LiAl/U-P FeS_2 and the FeS_2 electrode in the two-plateau monocell was the loading density. The 2-P cell had a density of 1.1 Ah/cm^3 while Kaun's cell had 2.4 Ah/cm^3. It was possible to increase the density of the FeS_2 electrode for upper-plateau operation because of the high density of the discharge product (Li_2FeS_2) [8]. Kaun's cell was designed for a cutoff voltage of 1.25 volts versus α-β LiAl [3], [7]; therefore, our model was never pushed past 48% depth of discharge.

Closed-circuit potential data for a current density of 50 mA/cm^2 were given by Kaun [3]. The corresponding apparent-open-circuit potentials of the cell were calculated from these data using Figure 8. The data points in Figure 9 were backed-out from these U_{cell} values using Figure 2.

The positive-ASR values were calculated by subtracting the negative-ASR values found in Figure 3 from the values found in Figure

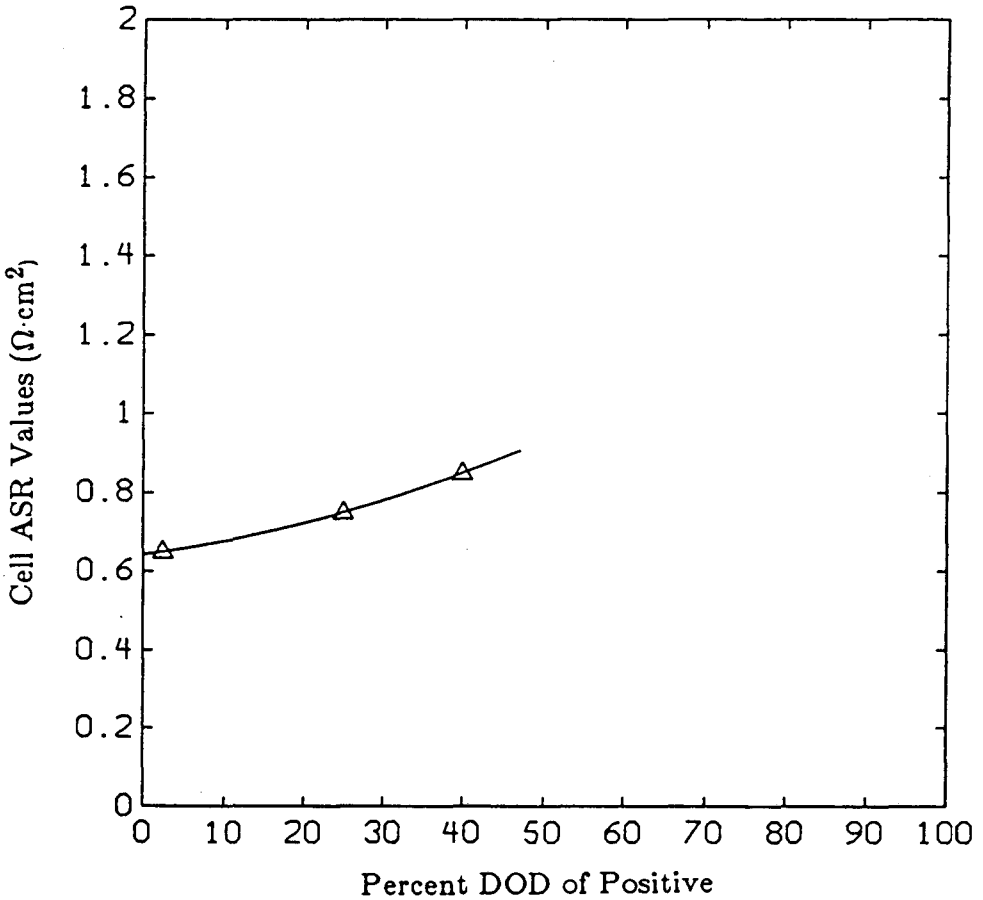

Figure 8. LiAl/Upper-plateau FeS_2 Cell Resistances. The curve fit stops at 48 percent DOD because the battery is never run beyond this point (data from reference 20).

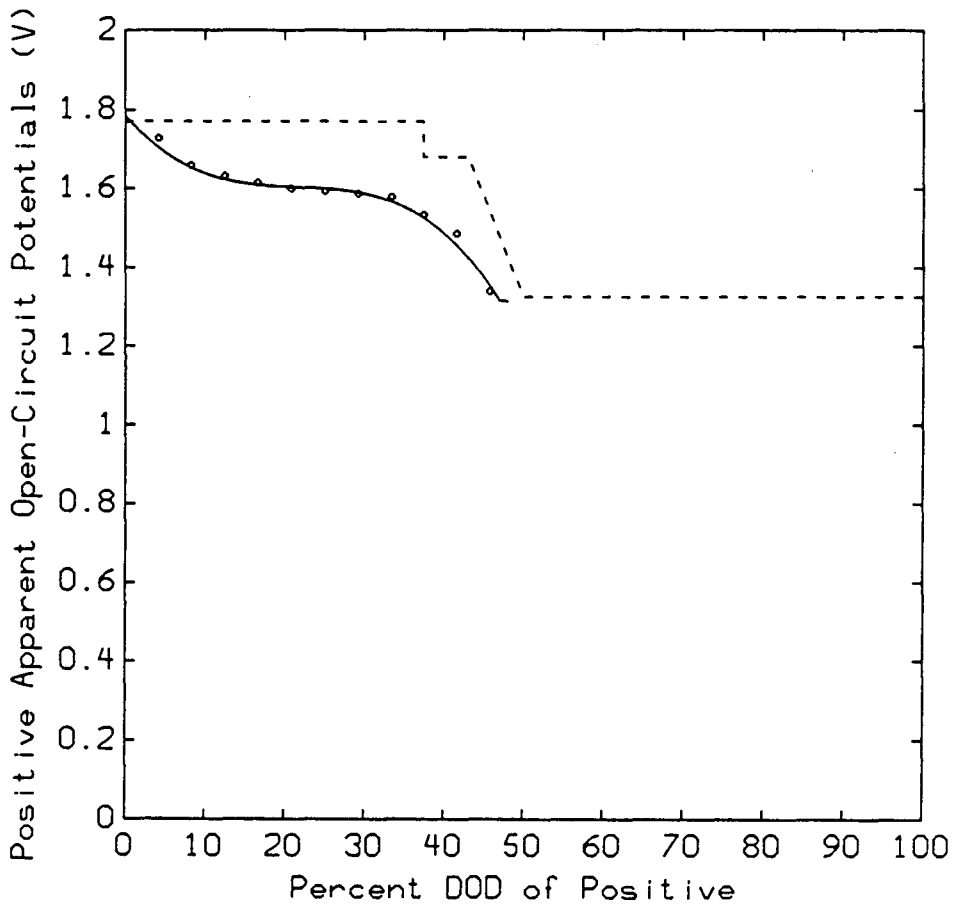

Figure 9. Upper-Plateau FeS_2 Potentials. The dashed line shows the thermodynamic open-circuit potential at 450°C (reference 2, p. 103). The curve fit (solid line) stops at 48 percent of *DOD* because is never run beyond this point. (Data calculated from reference 43, p. 1050, with figures 2 and 8.)

8. The U-P FeS_2 and 2-P FeS_2 closed-circuit potential curves at i=100 mA/cm^2 calculated from the curve fits given above were very similar.

2.3. Summary

Data from test cells that characterize the electrochemical behavior of certain battery systems were found. Curve fits of these data were combined with a mathematical model of the cells in order to calculate specific energy and specific power, as described below. The curve fits were placed in subroutines XPOS and XNEG in the computer programs (see Appendices A and B).

CHAPTER 3

Prismatic Cells

3.1. Optimization Procedure

The cells considered in this chapter had alternating positive and negative electrodes, as shown in figure 10. There were negative electrodes with one-half the normal thickness and capacity at the ends of the electrode stack. The ions that react in each positive half- electrode were imagined to have been transported from the separator that it faced, and each negative half-electrode discharged ions into its bordering separator. Thus, each positive electrode was associated with the two negative half-electrodes on either side of it.

The quantities that were optimized were specific energy and specific power. These quantities can be calculated as follows:

$$\hat{P} = \frac{U_{cell}^2}{4\,R\,W}\ , \tag{3-1}$$

$$\hat{E} = \frac{Q}{W} \cdot \int_{x=0}^{x=DOD} (U_{cell} - IR)\ dx\ , \tag{3-2}$$

where $\hat{P}$ is the maximum specific power (W/kg), $\hat{E}$ is the specific energy (J/kg), R is the internal resistance of the battery (Ω), I is current delivered (A), Q is the total capacity (C), W is the battery weight (kg). It has been assumed that the current-potential curve for the cell is a straight line and that, therefore, the maximum power available from the cell can be characterized by the apparent open-circuit

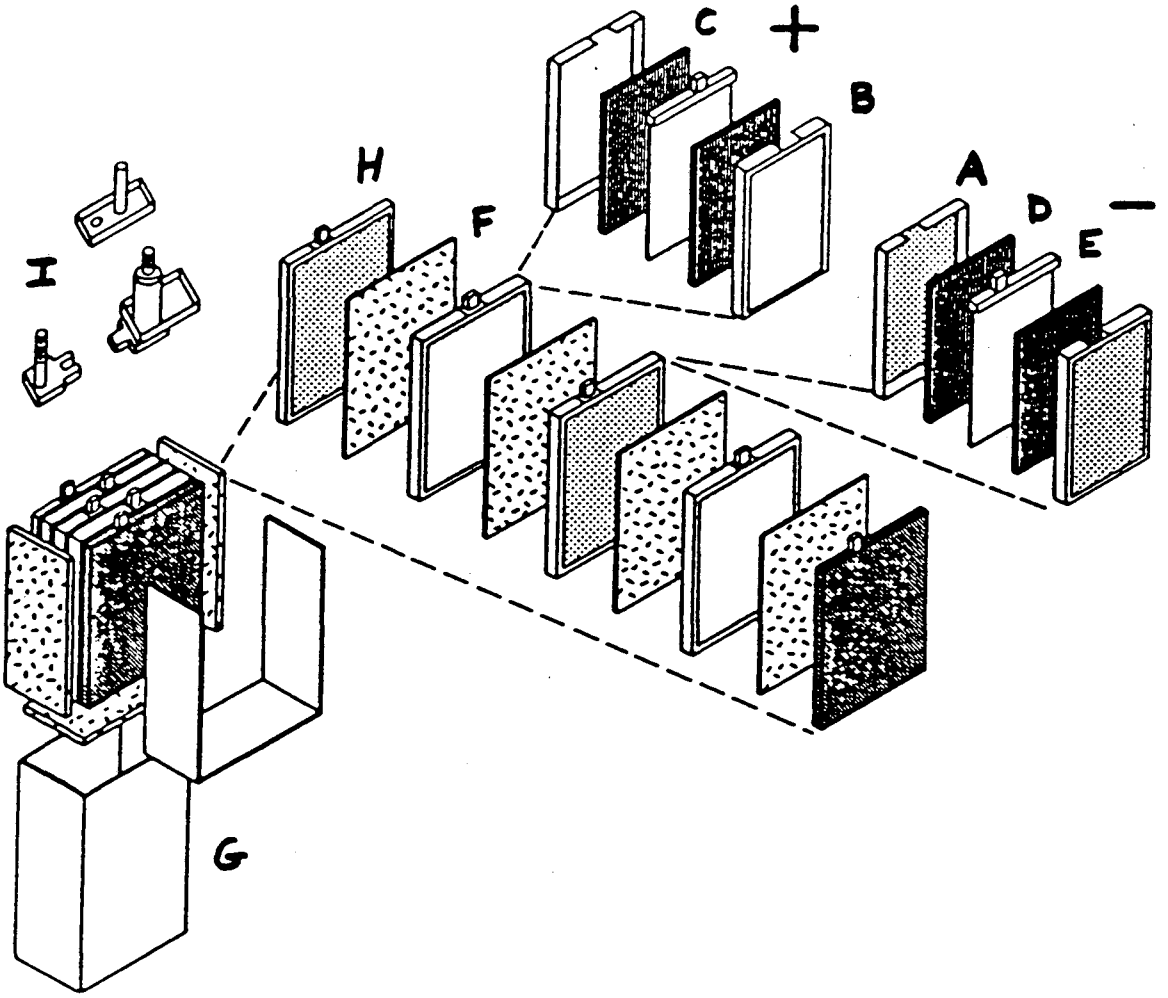

Figure 10. A prismatic cell design.

Taken from reference 5, p. 147.

A - negative electrode binder
B - positive electrode binder
C - positive active material (for example: FeS)
D - negative active material (LiAl)
E - current collector grid or sheet
F - separator (BN felt)
G - cell can
H - negative half-electrodes at end of stack
I - bus and post connectors

potential and the internal resistance. The apparent-open-circuit potential in these equations was given by the input data. The resistance was calculated from a combination of experimental ASR values and a mathematical model of the current collector grid, bus and post resistances.

We define a positive electrode unit as a combination of a positive electrode, the negative half electrodes facing it, and the included separators. It will be demonstrated that we can make the calculations given in Equations (3-1) and (3-2) using quantities on a per-positive-electrode basis.

Two common current-collector designs for prismatic batteries are sheet current collectors and grid current collectors. Trost presented a correlation between dimensionless electrode-plate conductance and dimensionless plate area for a current-collector grid [10] [11]. This correlation, which contains the experimental ASR as a parameter, was used in our model to approximate the combination of grid resistances and electrochemical resistances for a positive electrode unit.

The dimensionless plate-conductance correlation was used as an approximation in two situations where the current collectors were not grids. Some of the cells that were modeled in this work used an electrode binder as the current collector instead of the optimized grid. The correlation presented by Trost was used in these cases to approximate the resistance. The Li(Alloy)/FeS_2 cells require molybdenum current collectors; therefore, it is probable that sheet current collectors would be used instead of grids due to the relative ease of

fabrication. The correlation was used as an approximation in this case as well.

The correlation predicts the resistance due to the cell electrochemistry and the current collector grids. The interconnecting bus and post resistance also contributed to the overall cell resistance.

The current collector in each electrode was electronically connected to the appropriate post. We considered the sum of the negative and positive post resistances to be composed of N_{pos} (number of positive electrodes) larger resistances in parallel. Each one of these larger resistances was considered to be in series with a bus resistance and the sum of the electrochemical and grid resistances associated with a positive electrode unit. This series of resistances represented the total resistance associated with a positive electrode unit (R_{pos}). The resistance of each positive electrode unit acted in parallel with the other positive electrode units to give the overall battery resistance. It is possible to calculate the battery's specific energy and specific power using quantities on a per-positive basis by making the following substitutions into Equations (3-1) and (3-2):

$$W = N_{pos} W_{pos}$$

$$I = N_{pos} I_{pos}$$

$$Q = N_{pos} Q_{pos}$$

$$R = \frac{R_{pos}}{N_{pos}}$$

where the *pos* subscript refers to the positive electrode unit. The total resistance, R, is assumed to consist of N_{pos} individual resistances, R_{pos}, in parallel.

The following equations, which were presented by Trost [10], were used to calculate the optimum bus and post weights. The resistance of the bus and post combination will be denoted by R'. The value of R' optimized to yield the maximum specific power is

$$R'_{MaxP} = \left[\frac{R_{1/2}{}^{\delta}}{W_{base}}\right]^{1/2} , \tag{3-3}$$

where $R_{1/2}$ is the electrochemical plus grid resistance (Ω) halfway through discharge and W_{base} is the base weight of the positive electrode unit. W_{base} includes the weight of the grids, active material, electrolyte, a percentage of container weight, *etc.*, but not the weight of the bus and post. δ is given by

$$\delta = 0.004 \left\{ L_{bus}\left[\frac{\rho_{bus}}{\sigma_{bus}}\right]^{1/2} + L_{post}\left[\frac{\rho_{post}}{\sigma_{post}}\right]^{1/2} \right\}^2 . \tag{3-4}$$

This is equivalent to $\delta = R'W'/1000$ ($\Omega \cdot kg$) and $W' = W_{bus} + W_{post}$ (g). (W_{post}, here, is that part of the post associated with one positive electrode.) The two equations given above can be use to calculate R' and W' for maximum specific power. The optimum weight of the bus can be calculated from

$$W_{bus} = \frac{W'}{1 + \left(\frac{\sigma_{bus}\rho_{post}}{\sigma_{post}\rho_{bus}}\right)^{1/2}\left(\frac{L_{post}}{L_{bus}}\right)} \quad . \tag{3-5}$$

Finally,

$$W_{post} = W' - W_{bus} \quad . \tag{3-6}$$

The value of R' that optimizes for maximum specific energy takes the form,

$$R'_{MaxE} = \frac{\frac{1}{DOD}\int_0^{DOD}\left(\frac{U}{I} - R\right)dDOD}{1 + \left\{1 + \frac{W_{base}}{\delta DOD}\int_0^{DOD}\left(\frac{U}{I} - R\right)dDOD\right\}^{1/2}} \quad , \tag{3-7}$$

where R is the sum of the electrochemical plus grid resistance. The maximum energy and power optima are always bounded by the constraint that the cell voltage can never fall below the cut-off voltage. For any depth of discharge the cut-off voltage can always be reached by setting R' to

$$R'_{cut} = \frac{(U - V_{cut})}{I} - R \quad , \tag{3-8}$$

Trost showed how to calculate a value of R' such that the resulting power to energy ratio is equal to a value selected as a compromise ratio. Here R' is the solution of the quadratic equation

$$AR'^2 + BR' + C = 0 \quad , \tag{3-9}$$

where

$$A = I \cdot DOD \quad , \tag{3-10}$$

$$B = AR_{1/2} - \int_0^{DOD} (U - RI)\,dDOD \quad , \tag{3-11}$$

and

$$C = \frac{U^2}{4Q \cdot (RATIO)} - R_{1/2} \int_0^{DOD} (U - RI)\,dDOD \quad , \tag{3-12}$$

where *RATIO* is the desired ratio of power to energy.

The computer program (see Appendix A) consists of three basic parts. The first part incorporates the subroutines that contain the curve fits of the experimental data. This part also includes a subroutine that uses the correlation given by Trost to calculate the combined electrochemical and grid resistances. The second part contains the input statements for battery design parameters (number of electrodes, capacities, *etc.*). These parameters are then used to size the battery and to calculate the weights of the various battery components. The bus and post weights and R' are calculated using Trost's equations. These values are used to calculate the specific energy and specific power of the battery in the third part of the program.

The program can be used to examine the effect that changing a design parameter has on specific energy and specific power. Optimum values of various design parameters can be found in this manner.

3.2. Results and Discussion

The negative-to-positive capacity ratio can be optimized because a trade-off exists between potential and weight. The potential of the LiAl negative increases with added utilization (see figure 2); therefore, the battery voltage at a given percent of positive utilization

is increased if the capacity ratio is increased. The higher-voltage advantage gained by adding negative active material is accompanied by an increase in the battery weight. In addition to the added weight of active material there is a weight gain caused by the increased volume of the negative electrode (*e.g.*, heavier current collector).

In the past, when LiAl electrodes were cold-pressed, it was necessary to have at least a 1.3 negative-to-positive capacity ratio because the rate of capacity decline of the LiAl electrode increased significantly at utilizations beyond 65 percent of the theoretical capacity [1]. More recently, LiAl electrodes fabricated by a slurry method have demonstrated stable operation at utilizations approaching 80 percent [3]. These slurry-formed electrodes have permitted the development of Li-limited LiAl/FeS batteries.

A model based loosely on a multiplate-cell design developed by Gould, Inc. [5], [21], was used to examine the effect of capacity ratio on LiAl/FeS cell performance. In this design the electrodes were contained within a "picture frame" assembly, as shown in figure 10. Our model of this "picture frame" consisted of a 0.01 cm thick metal strip (Fe for positive and 1008 steel for negative) that surrounded the perimeter of the electrode and held a screen (55% open area) on each face of the electrode. The weight of material required for this electrode enclosure was considered to be the minimum current-collector weight. In a separate optimization of current-collector weight, it was determined that this minimum weight was heavier than the weights required for maximum specific energy and

power. Therefore, the current collector weight was set equal to this minimum. In the cell design, strips of felt material were placed at the base and sides of the cell container to prevent short circuiting. The weights of these were neglected in the model. Some model parameters are given in Appendix D.

The positive-electrode thickness was 0.35 cm. The computer program adjusted the electrode area so that 30 Ah were delivered in four hours. Various capacity ratios were achieved by varying the negative-electrode thickness (0.54 cm to 0.67 cm), and the effect of electrode thickness on the negative ASR values was ignored. The bus and post resistances were also ignored. This model was employed to demonstrate how our method can be used to optimize cells; it was not based on the design of a cell that was being developed simultaneously.

Figure 11 shows results for the LiAl/FeS system. There is a maximum in specific energy at 1.2 Ah of negative capacity per Ah of positive capacity.

Similar curves were obtained for the LiAl/2-P FeS_2 and the LiAl/U-P FeS_2 cells with the maximum specific energies at 1.1 and 0.7 Ah neg./Ah pos. respectively. The models used for these cells were identical to the LiAl/FeS model except that the positive-current collectors were made of molybdenum. The optimum-capacity ratio of the upper-plateau FeS_2 cell was small because less than half the positive capacity was used during discharge.

Having explored the effect of capacity ratio on cell performance, comparisons between the LiAl/FeS, LiAl/2-P FeS_2, and LiAl/U-P FeS_2

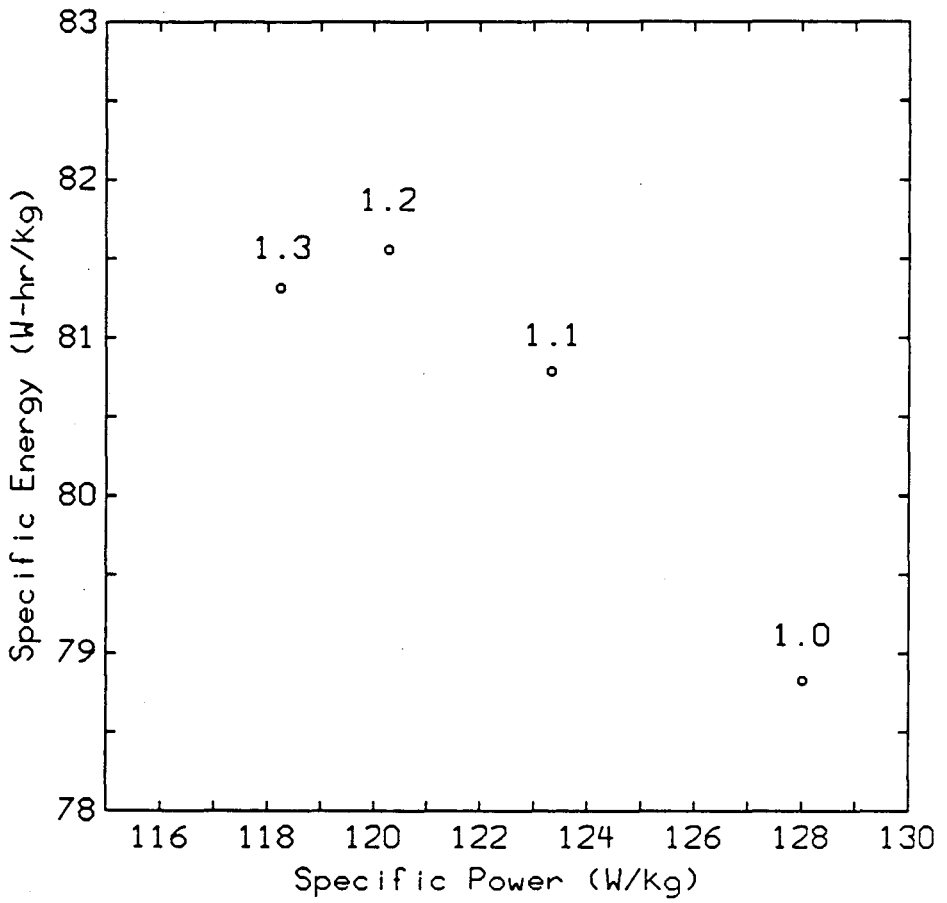

Figure 11. Effect of Negative-to-positive Capacity Ratio on Energy and Power. Specific energy and specific power for a LiAl/FeS battery with different capacity ratios.

systems were made. Table 1 gives a description of the three batteries whose capacity ratios were optimized for maximum specific energy. Additional results from the simulations are presented in Appendix E. In each case the energy per kilogram of positive active material was about 80 percent of the theoretical value. The theoretical-energy per kilogram was calculated from Equation (3-2) by setting R equal to zero, Q/W equal to the theoretical capacity per kilogram of positive active material, and DOD equal to one (FeS and 2-P FeS_2) or one-half (U-P FeS_2).

The specific energies calculated from the model do not correlate with the energies per kilogram of positive active material because the percent of the total weight due to the positive active material was different for each system. There were several reasons for this. The capacity ratio was different for each system (1.2 for FeS, 1.1 for 2-P FeS_2, and 0.7 for U-P FeS_2). The loading density of the positive active material was also different for each system (1.4 Ah/cm^3 for FeS, 1.5 Ah/cm^3 for 2-P, and 2.4 Ah/cm^3 for U-P). The volume percent of electrolyte was higher for electrodes with smaller densities. In addition, the electrodes with smaller densities required more volume, and the additional volume resulted in a need for more cell-hardware mass (*e.g.*, current-collector mass).

The specific energies and specific powers predicted by this model were less than those that have been achieved experimentally [3] because the cell design that was modeled is less effective than more recent designs. For example, Kaun [18] described a LiAl/FeS cell

Table 1. Comparison of Various Optimized Battery Systems

	LiAl/FeS	LiAl/2-P FeS_2	LiAl/U-P FeS_2
Cutoff Voltage (volts)	0.9	0.9	1.25
Percent DOD	89	84	45
Theoretical E/kg pos. (W-hr/kg)	814	1267	760
Model E/kg pos. (W-hr/kg)	652	997	617
Model Specific Energy (W-hr/kg)	82	96	93
Model Specific Power at end of DOD (W/kg)	33	40	140
Percent of total weight due to pos. active material	12.5	9.7	15.1

where the weight contribution of the electrode materials was 36% of the cell weight, as opposed the 23% for this model.

The advantage of using a LiAl/U-P FeS_2 cell is demonstrated clearly in figure 12. The specific energies fall within an 18 W-hr/kg range, but specific powers (at 50% DOD) cover a 150 W/kg range. Table 1 shows that the LiAl/U-P FeS_2 cell has more than three times the power available at the end of discharge as the other two. The choice of which cell is best for a given application depends strongly upon the power requirements of the application.

Economies of scale are important in load-leveling, where cells can have a total available energy on the order of 1 kW-hr [22]. As the cell size increases, one will want to consider how many electrodes to use.

A model of a LiAl/U-P FeS_2 cell was used to examine the effects of capacity and the number of electrodes on cell performance. The model was similar to the ones used previously, except that the bus and post resistances were included. The posts were made out of iron and had a length of 2 cm. The busses were also constructed from iron, but the lengths varied according to the distances between the electrodes and the posts. The bus and post weights were optimized for maximum specific energy.

Figure 13 presents results for various capacities and numbers of positive electrodes. For the range of capacities presented here, the specific energy and specific power increased with cell capacity because the active materials constituted a higher fraction of the

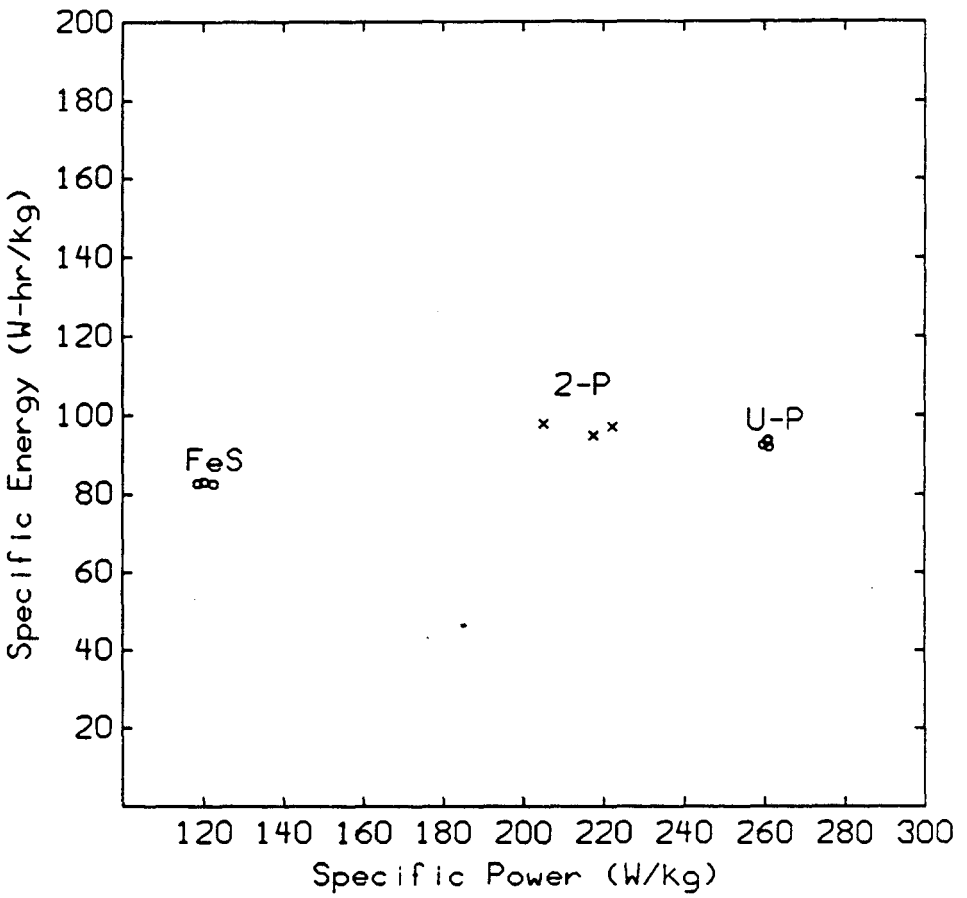

Figure 12. Comparison of Various Battery Systems. Comparison of LiAl/FeS, LiAl/2-P FeS_2, and LiAl/U-P FeS_2 battery systems. Different points represent different negative-to-positive capacity ratios. Specific power is at 50 percent *DOD*.

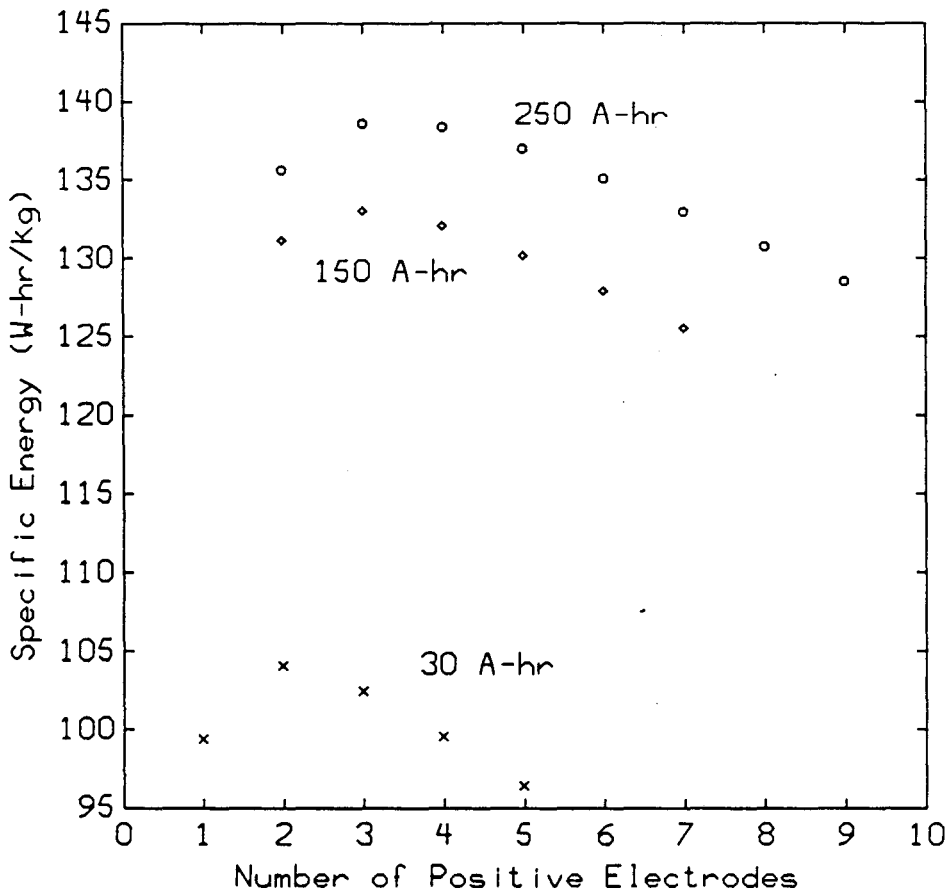

Figure 13. Effect of the Number of Positive Electrodes and Total Cell Capacity on Specific Energy. The bus and post weights of a LiAl/U-P FeS_2 cell are optimized for maximum specific energy.

overall weight. During an increase in capacity, the surface area and, hence, the cell-can weight increased more slowly than the weight of active materials. The current-collector weight was increased with electrode capacity so that IR drop was not an important factor.

The optimum number of positive electrodes (N_{pos}) increased with cell capacity. This was the result of several factors acting simultaneously. The bus resistances increased with N_{pos} because of their increased length. The plate area decreased as N_{pos} increased, and this decrease in plate area caused the grid resistance to decrease. The can weight was a function of N_{pos}:

$$CANWT = (\rho_c)(L_c)\left\{\frac{2A_t}{N_{pos}} + 4L_t\sqrt{A_t N_{pos}}\right\}, \qquad (3\text{-}13)$$

where A_t is the total area of all the positive electrodes (cm^2), L_c is the thickness of the can (cm), ρ_c is the density of the can material (g/cm^3), and L_t is the total thickness of one positive electrode, one negative electrode, and two separators (cm). The can weight went through a minimum as N_{pos} increased; the minimum was at larger values of N_{pos} for larger total electrode areas (*i.e.*, capacities). These three factors, acting simultaneously, resulted in an optimum N_{pos}, which increased with increasing capacity. The optimum N_{pos} would be even higher at large capacities if it were not necessary to increase the bus length as N_{pos} increased.

3.3. Conclusions

The approach presented in this chapter allows one to examine the trade-off between specific energy and specific power for different

capacity ratios. The negative capacity should be matched with the positive capacity so that the desired performance is achieved.

The theoretical energy per gram of positive active material of LiAl/2-P FeS_2 is much greater than LiAl/FeS or LiAl/U-P FeS_2. However, the practical specific energies are all very close (within 15%).

The LiAl/U-P FeS_2 cell has much better power characteristics than the other two cells.

The model can be used to optimize the number of positive electrodes for a given cell capacity. The optimum N_{pos} increases with increasing cell capacity for the cell design used in this paper.

The cell optimizations that have been considered in this work are not independent. Materials of construction and ease of fabrication also need to be considered in cell design. Despite these limitations, this approach provides a battery designer with the ability to explore various design alternatives and screen potential systems before actually constructing a scaled-up cell.

CHAPTER 4

Cylindrical Cells

4.1. Mathematical Model

Nelson *et al.* [9] described the cell design modeled here. The cell is illustrated in Figure 14. The cell container is cylindrical and acts as a current collector for the LiAl. This cell contains a plurality of positive electrodes. Each positive electrode has an elongated pin shape and includes a molybdenum-rod current collector at its center. The positive material is surrounded by a separator, and the whole electrode unit is contained within a perforated tube that acts as a negative current collector. LiAl fills the voids around the positive electrode units. A metal disk serves as a bus and interconnects each of the positive current collectors with a common cell terminal. The terminal extends through, but is electrically insulated from, the top end of the container. Insulators and structural supports are used as needed. Some model parameters are given in Appendix D.

The model is based on the assumption that the ionic current that travels between the negative and positive active materials only travels in the radial direction. In other words, an equal number of coulombs enter and leave a separator at a given height, and the extent of reaction is uniform across the whole cell at a given height. This assumption allows us to use one-dimensional micro-models or data from

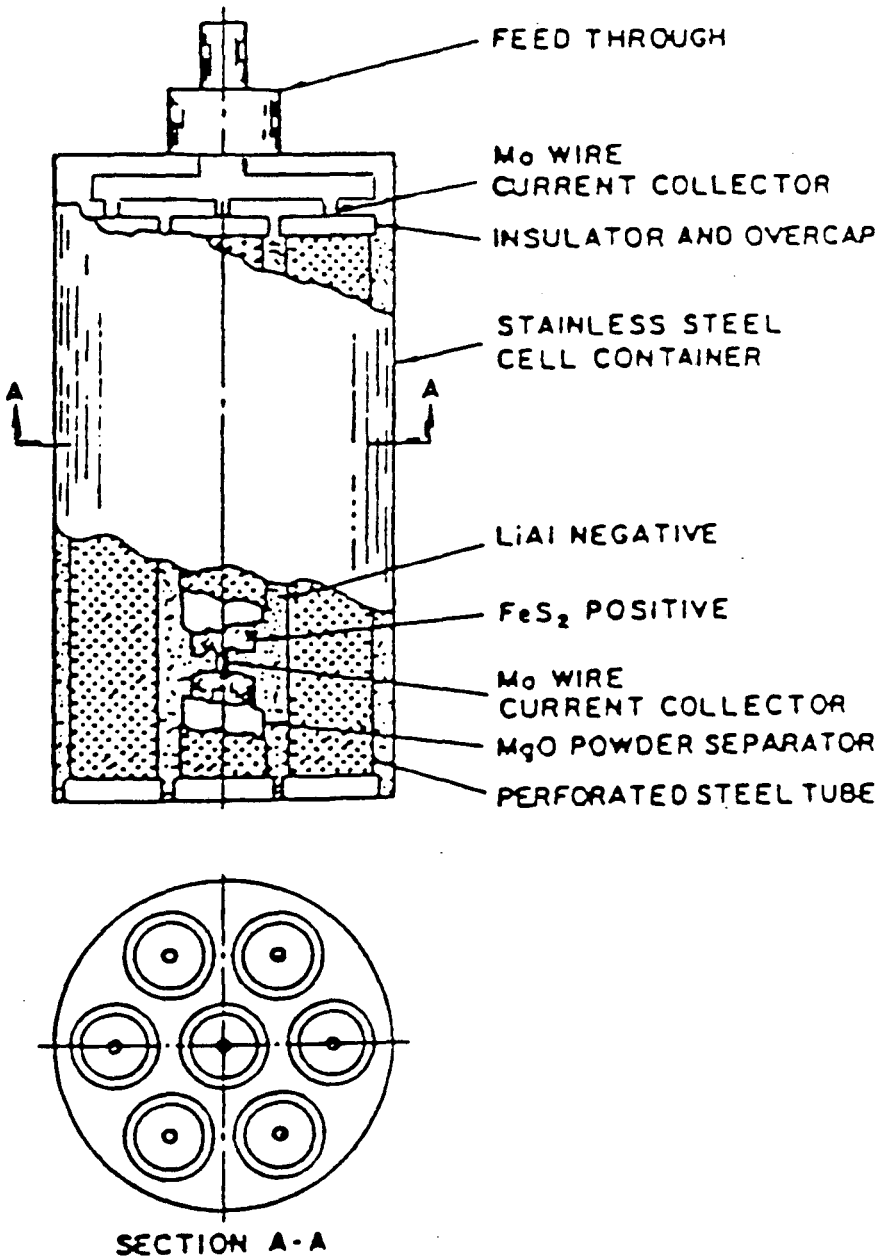

Figure 14. Schematics of cylindrical cell design. Reproduced from reference 3, p. 1090, with minor alterations.

one-dimensional test cells to predict the current-potential relationships for the electrochemical reactions. A one-dimensional micro-model could describe the detailed processes that occur within and between the electrodes: reaction kinetics, transport phenomena, and structural changes. In this work experimental data from prismatic one-dimensional test cells were used to characterize the electrochemical behavior of the cell.

In the experimental, prismatic test cells, the current density was the same at each plane that was perpendicular to the direction of current flow. Using data from these test cells introduced error into the model because current densities vary with radial position in cylindrical cells; however, we resorted to this procedure because we lacked more appropriate data.

The model was used to calculate specific energy and specific power. These quantities can be calculated as shown in Equations (3-1) and (3-2). The overall resistance was calculated from a combination of experimental ASR values and the mathematical model of the other resistances in the cell. The other resistances were due to the current collector and the interconnecting bus and post.

We focused on the positive current collector design by neglecting the resistance of the negative current collector. The current collector resistance can be accounted for by making a shell balance, which leads to the following equation:

$$\pi r_i^2 \sigma \frac{d^2\phi}{dy^2} + \frac{2\pi(r_o - r_i)}{ASR \cdot \ln(r_o/r_i)}(U-\phi) = 0 \ , \qquad (4\text{-}1)$$

where ϕ is the potential of the positive current collector with respect to the zero potential negative current collector (volts), r_i is the outer radius of the positive current collector (cm), r_o is the outer radius of the separator (cm), y is the height from the bottom of the current collector (cm). The separator area in Equation (4-1) has been based on a logarithmic mean radius:

$$A = \frac{2\pi H}{r_o - r_i} \ln(r_o/r_i) \ , \qquad (4\text{-}2)$$

were H is the separator height (cm). The differential equation is subject to the following boundary conditions:

$$\frac{d\phi}{dy} = 0 \qquad at\ y=0 \ , \qquad (4\text{-}3)$$

$$I = -\pi r_i^2 \sigma \frac{d\phi}{dy} \qquad at\ y=H \ , \qquad (4\text{-}4)$$

where I is the total current that is delivered by the electrode (A).

Initially, all of the active material is fully charged, and U and ASR are not functions of height; consequently, the solution of Equation (4-1) is:

$$\phi(y;t=0) = U - \frac{I\alpha}{\pi r_i^2 \sigma}\left[\frac{\cosh(y/\alpha)}{\sinh(H/\alpha)}\right] \ , \qquad (4\text{-}5)$$

where

$$\alpha^2 = \frac{r_i^2 (ASR)\sigma \ln(r_o/r_i)}{2(r_o - r_i)} \ , \qquad (4\text{-}6)$$

where $\phi(y;t=0)$ is the potential of the positive current collector at y at the beginning of discharge with respect to the negative current

collector (V). The initial resistance of the electrode is given by:

$$R = \frac{U - \phi(H;t=0)}{I} , \tag{4-7}$$

$$R = \frac{\alpha}{\pi r_i^2 \sigma \tanh(H/\alpha)} , \tag{4-8}$$

where $\phi(H;t=0)$ is the potential at the top of the current collector with respect of the negative current collector (V). The penetration depth is given by the parameter α. For all values of H/α greater than one, the hyperbolic tangent term is approximately equal to one. Therefore, increasing H does not significantly decrease R.

The local reaction rates are nonuniform along the length of the positive current collector because the potential varies with height. The area-specific resistance varies along the length of the electrode because it is a function of the percent of active materials utilization. Therefore, at any time after $t=0$, both U and ASR in Equation (4-1) will be functions of height (y), and the differential equation will need to be solved numerically. In a time-stepping scheme the results from the previous time step could be used to determine the percent utilization of active materials at a given height by using Equation (2-2).

An alternative procedure is based on the assumption that there is only a small range of ASR values on the current collector at a given time. Equation (4-5) can then be employed at all times by using the average ASR value, which can be determined since the total discharge current and the amount of active materials is known. This procedure was used in this work.

The positive current collectors were electronically connected to each other and to the post by an interconnecting bus (see Figure 15). The post resistance is simply given by:

$$R_{post} = \frac{L_{post}}{\sigma \pi r_{post}^2} , \tag{4-9}$$

where L_{post} is the length of the post (cm) and r_{post} is the radius of the post.

We propose two ways of modeling the bus resistance. Figure 16 gives two top views of the post and a positive current collector. Consider the resistance between the positive current collector and the post. The schematic in Figure 16a can be used to calculate an upper bound for this resistance, and Figure 16b will provide a lower bound. Using Figure 16a to calculate the resistance gives

$$R_{bus} = \frac{\ln(2d/r_i)}{\sigma T \theta} \tag{4-10}$$

where θ is the angle between the hypothetical insulators (radians), r_i is the radius of the positive current collector (cm), T is the thickness of the bus (cm), and d is half the distance between the center of the current collector and the center of the post (cm). We use a coordinate transformation suggested by Adams [23] to find the resistance in Figure 16b:

$$R_{bus} = \frac{\gamma + \beta}{2\pi\sigma T} , \tag{4-11}$$

where

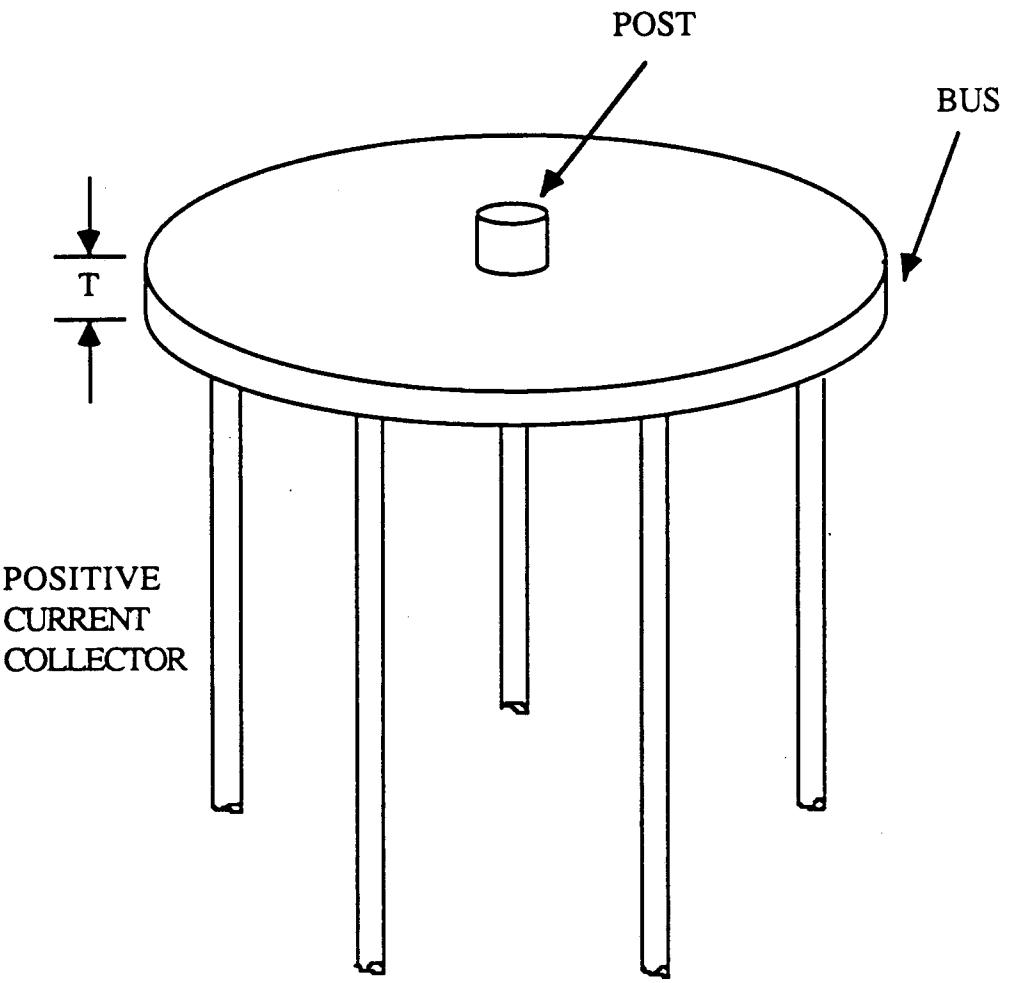

Figure 15. Schematic of the interconnecting bus

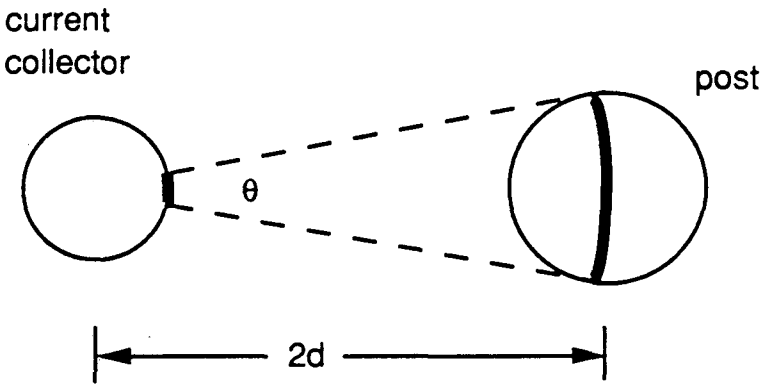

a. Upper Bound

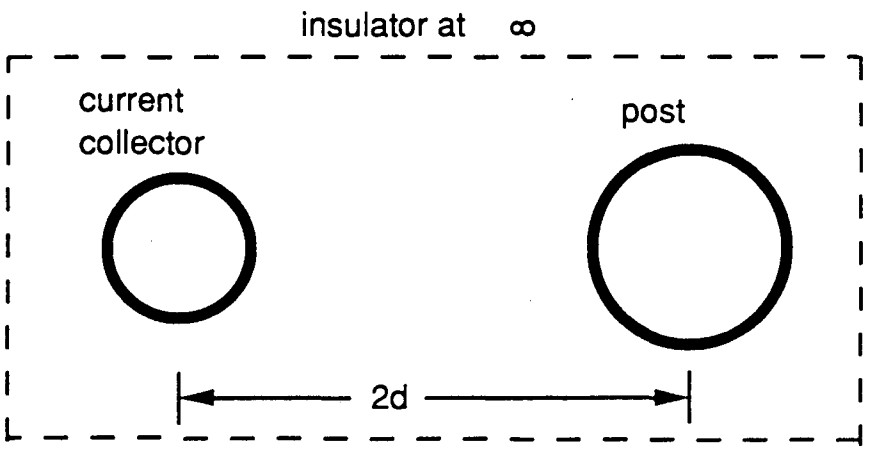

b. Lower Bound

Figure 16. Schematics for Calculating the Bus Resistance.
The dashed lines represent insulators.
The bold lines represent equipotential surfaces.

$$\gamma = \text{csch}^{-1}\left[\frac{r_i}{f}\right] , \tag{4-12}$$

$$\beta = \text{csch}^{-1}\left[\frac{r_{post}}{f}\right] , \tag{4-13}$$

and f is given by

$$2d = \left[r_i^2 + f^2 \right]^{1/2} + \left[r_{post}^2 + f^2 \right]^{1/2} . \tag{4-14}$$

There is a bus resistance in series with each electrode resistance, and this combination is in parallel with the other electrode-bus resistance combinations.

4.2. Results and Discussion

Table 2 describes some of the cell components used in the model. The discharge time was four hours, the cutoff voltage was 1.25 volts, and the negative to positive capacity ratio was 0.729 Ah negative/Ah positive. The computer program sized the various cell components and calculated the total cell weight based on three input parameters: the number of positive electrodes, the radius of the positive electrode current collector, and the height of the cell. Because the thickness of the positive electrode was set at a specific value, various combinations of positive current collector radius and cell height gave the same cell capacity. These combinations were evaluated for a 35 Ah cell and a 250 Ah cell. We could have changed the positive electrode bed thickness as well as the current collector design; however, this would have changed the electrochemical behavior of the cell, and the input data would need to reflect the change. For any reasonable

Table 2. Description of model parameters.

Component	Thickness, cm	Material	Density, g/cm^3
positive current collectors	...	Mo	10.2
positive electrode	0.4	FeS_2	2.68
separators	0.2	MgO	1.91
negative current collectors	0.0117	1008 steel	7.86
negative electrode	...	LiAl	1.04

number of electrodes, the optimum current collector radius was on the order of 0.1 cm. At this optimum radius the current density varied by a factor of five in the positive electrode, which had a bed thickness of 0.4 cm. This result is disappointing because it means that the literature data that we have been able to find are not appropriate for use with this model. The data discussed in the previous section were collected in a prismatic cell where the current density did not change across the thickness of the positive electrode. In order to improve this model, data from cylindrical test cells are needed.

The purpose of the computer simulations discussed above was to determine if the available electrochemical data could be used to predict cell behavior accurately. Therefore, the resistances of the bus and post were not included in the program. It has been shown that the data required to obtain accurate results are not available. For this reason, the program was never altered to account for the bus and post resistances. However, Equations (4-9) and (4-14), which can be used to calculate these resistances, were presented in the discussion of the mathematical model so that they can be used when more appropriate data become available.

Although the appropriate data are not available for accurate modeling of the $LiAl/FeS_2$ cell, the model was used to estimate optimum current collector designs and to examine the effect of changing the number of electrodes in a cell. This type of approach could help guide initial battery development efforts.

Figure 17 presents results for a cell with 35 Ah theoretical capacity and four positive electrodes. The points in Figure 17 show the specific energy and specific power at 80 percent depth of discharge (*DOD*) of cells with different combinations of positive current collector radius and cell height. The weight of the current collector increased as the current collector radius increased. Lighter current collectors favored specific energy, and heavier, lower resistance current collectors favored specific power.

The number of positive electrodes in the cell (N_{pos}) is another design parameter that can be optimized. Figure 18 shows the effect of N_{pos} for a cell with a 250 Ah theoretical capacity. Each point represents the current collector radius and cell height combination that gave maximum specific power. Figure 19 gives the results for cells whose current collectors were optimized for maximum specific energy. Both sets of results initially exhibit a sharp rise, then level-off, and eventually start to decline. The dominant factor causing this behavior was the variation of cell weight as N_{pos} increased. The cell weight experienced a rapid decrease, then a leveling-off, and finally an increase as N_{pos} increased. The weight minimum was found in the same region as the specific energy and specific power maxima. The change in weight was due to changes in the separator, negative current collector, and cell container weights as the radius and height changed. The cell resistance influenced the cell behavior to a lesser degree than the cell weight. Although the resistance of individual electrodes increased as N_{pos} increased, the total resistance of all

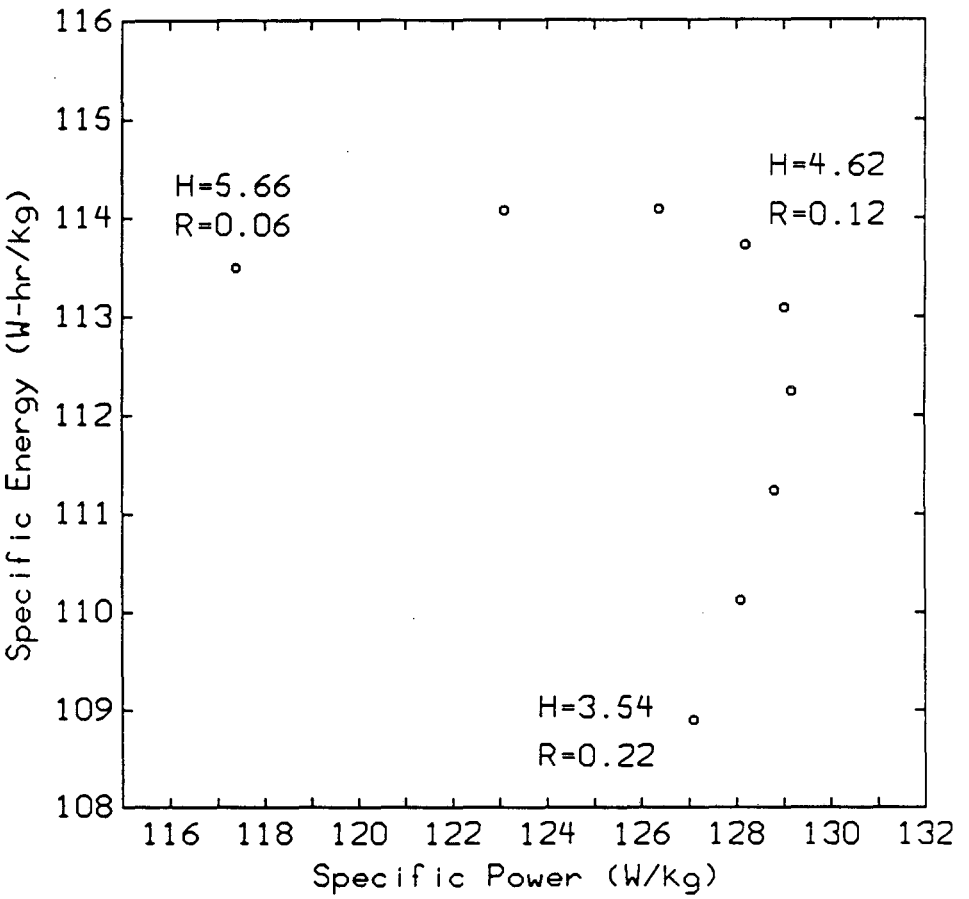

Figure 17. Effect of Positive Current Collector Design. The points represent different combinations of current collector radius (R) and height (H) that gave a 35 Ah theoretical capacity. The specific power is the maximum available at 80% DOD. The cell had four positive electrodes, each with a 0.4 cm thick bed of active material. The discharge time was four hours.

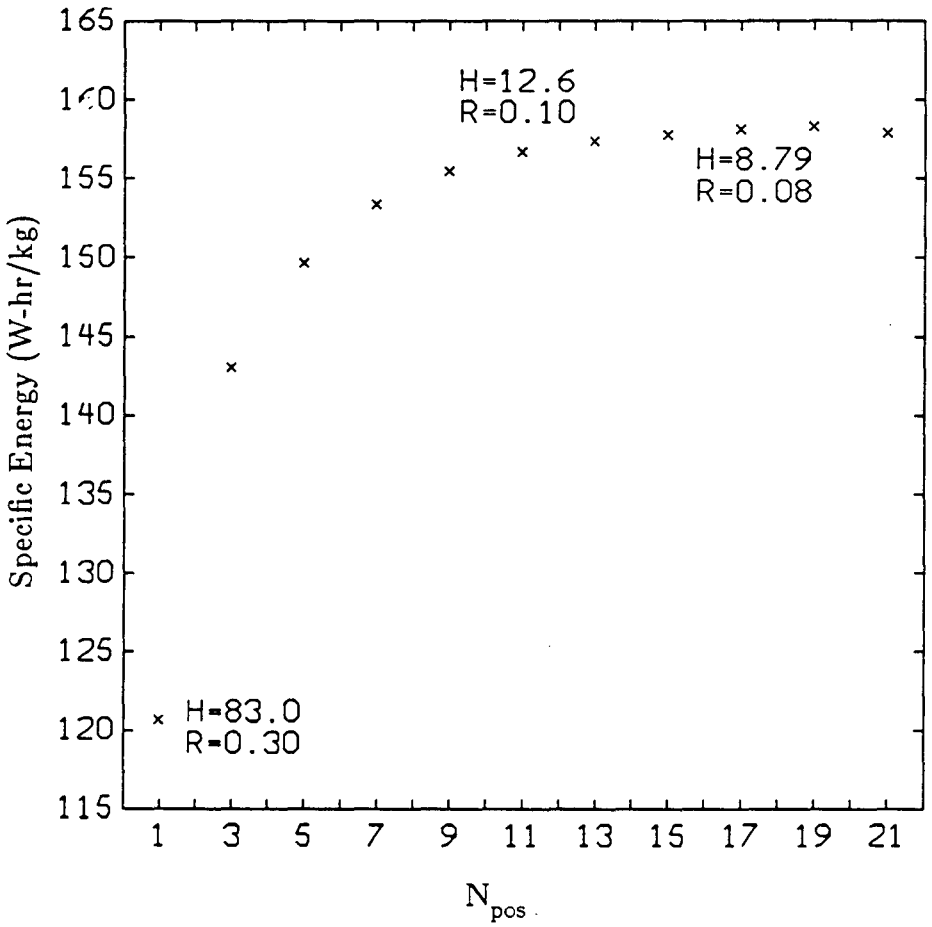

Figure 18. Effect of the Number of Positive Electrodes on Specific Energy. The current collector height (H) and radius (R) were selected at each point so that the cell was optimized for specific energy and the theoretical capacity of the cell was 250 Ah. The discharge time was four hours.

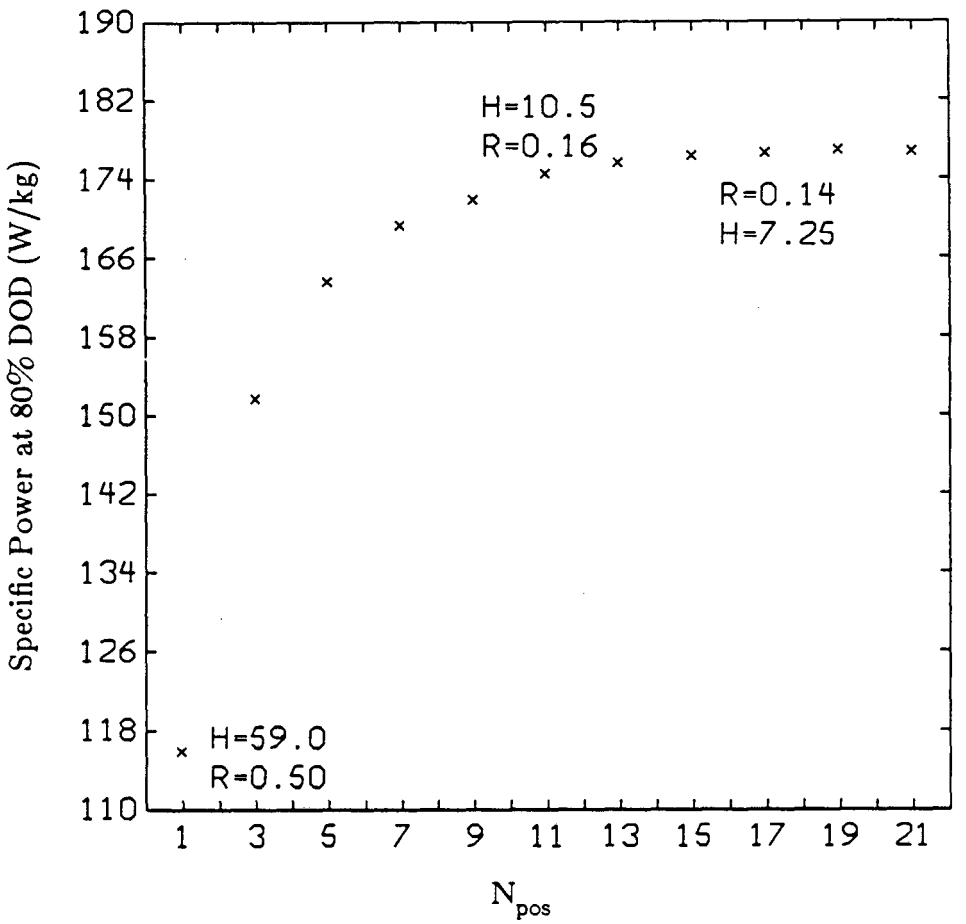

Figure 19. Effect of the Number of Positive Electrodes on Specific Power. The current collector height (H) and radius (R) were selected at each point so that the cell was optimized for specific power and the theoretical capacity of the cell was 250 Ah. The discharge time was four hours.

the electrodes in parallel decreased.

The results given in figures 18 and 19 come from simulations that do not account for the bus and post resistances; therefore, it is important to consider how these resistances will affect the cell behavior. The bus and post resistances would cause additional voltage losses that would lower the specific energy and specific power. As the number of electrodes increased, the size of the bus would need to be increased and, consequently, the bus resistance would increase. The bus resistance would have more effect at higher values of N_{pos}. The packing arrangement used for the electrodes would determine how large the bus needed to be.

Table 3 shows the optimum cell design for the 250 Ah cell. Eleven electrodes were chosen as the optimum number of electrodes because, as can be seen in figures 18 and 19, very little specific energy or specific power is gained by using a larger number of electrodes. The results from a similar optimization of a 35 Ah cell are also given. These results could be used to guide initial attempts to develop a multi-tube LiAl/FeS_2 battery.

4.3. Conclusions

A model for a multi-electrode cylindrical cell has been presented that can be used to predict cell behavior and optimize cell design parameters. It has been shown that data from prismatic test cells cannot be used to model accurately the LiAl/FeS_2 cylindrical cell because the current densities vary too much in the radial current dis-

Table 3. Optimum Cell Designs for Maximum Specific Energy and Maximum Specific Power for a Cylindrical Cell.
A LiAl/U-P FeS_2 cell has been optimized. Pos. cc. is an abbreviation of positive current collector. The rows labeled N give the number of positive electrodes in the cylindrical cell. The cell optimized for maximum power is optimized for maximum power at 80 percent depth of discharge.

		Total Capacity (Amphere-hours)	
		35	250
Maximum Specific Energy	N	5	11
	height	4	13
	pos. cc. radius (cm)	0.08	0.10
	can radius (cm)	2.18	3.31
	Sp. E. (W-hr/kg)	114	157
	Sp. P. (W/kg)	124	167
Maximum Specific Power	N	4	11
	height	5	11
	pos. cc. radius (cm)	0.16	0.16
	can radius (cm)	2.90	3.61
	Sp. E. (W-hr/kg)	112	154
	Sp. P. (W/kg)	129	174

tribution. In spite of this fact, the model has been used to make preliminary estimates of optimum cell designs. Once data are available that characterize the electrochemical behavior of cells with radial current distributions, the model presented here could be used to guide the development of cylindrical batteries.

CHAPTER 5

Electronic Conductivities in Porous Electrodes

5.1. Introduction

This chapter could be called a 'future work' chapter. Its purpose is to describe a problem that has arisen from Li(Alloy)/FeS_x cell modeling efforts. Although no progress has been made towards solving this problem, a review of some of the pertinent literature is given. It is hoped that this chapter will give a future researcher a basis for proceeding to solve this problem.

The FeS_2 and FeS electrodes can be described as unconsolidated, heterogeneous mixtures of solids in slurries with molten-salt electrolytes. On a macroscopic level, different parts of an electrode can have different compositions because the reaction rates are not uniform throughout the electrode volume. On a microscopic level, the chemical composition and the microstructure will change during charge or discharge. Researchers at Argonne National Laboratory have presented photomicrographs of the electrodes in Li(Alloy)/FeS_x cells [24], which show these changes.

Mathematical models of Li(Alloy)/FeS_x cells were presented by Pollard [25] and Bernardi [2]. These models incorporate porous electrode theory that was reviewed by Newman and Tiedemann [26]. An effective conductivity is used to describe the flow of electrons through the solid matrix phase. This quantity is affected by the

volume fraction of the conducting phase or phases, the inherent conductivity of each conducting solid phase, and the manner in which granules of conduction phases are connected together [26]. Both Pollard's and Bernardi's models predicted lower positive electrode resistances than those observed experimentally. Newman [27] asserted that discrepancies between model and experimental results can be attributed to poor approximations to the effective conductivity of the electrodes. Thus, a method for predicting the effective conductivities of these packed-bed electrodes needs to be found.

A model that can aid in development and optimization of a multi-electrode, cylindrical LiAl/FeS_2 cell was presented in Chapter 4. Unfortunately, I was unable to find the data required to characterize the electrochemical behavior of the active materials. If a one-dimensional micro-model were available to describe the electrochemical behavior, then it could be coupled to the model presented earlier, and the need for experimental data would be eliminated. In addition to being able to model accurately these molten-salt batteries, there are other possible benefits to studying the effective conductivities of heterogeneous mixtures. One might be able to optimize an electrode using the increased understanding of how electrons are transported through the solid matrix. The theory that would be developed might be applied to predicting effective transport coefficients for other physical phenomena, such as heat conduction or magnetic permeability.

5.2. A Literature Review

The literature pertaining to transport in heterogeneous media is huge. The goal of this chapter is not to present an exhaustive review of the literature but to discuss some selected papers and to put things into perspective.

A large variety of substances can be classified as heterogeneous media. The differences between the conductivities of the component phases can be very small (metal alloys) or very large (insulating inclusions in a conducting matrix). The concentrations of the components can cover a large range of values, from very disperse, small inclusions in a continuous matrix (*e.g.* gas bubbles in electrolytic solution) to either an unconsolidated mixture of solid particles or a sintered porous material.

The effective conductivity is rigorously defined by

$$\mathbf{i} = \underline{\sigma}^* \mathbf{E} \quad , \tag{5-1}$$

where $\mathbf{i}$ is the average current flow, $\underline{\sigma}^*$ is the effective conductivity tensor, and $\mathbf{E}$ is the average electric field. The effective conductivity is a scalar if the medium is isotropic over the length scale being considered. In this case,

$$\mathbf{i} = -\sigma^* \nabla\phi \quad . \tag{5-2}$$

The effective conductivity is a function of the conductivities of the individual components and the structural detail of the medium. The proportionality constant between a flux density and an associated field can define other effective transport properties in addition to

conductivity. However, the phenomena determining the individual pure-phase transport coefficients must have a shorter length scale than the length scale of the heterogeneities of the medium.

It is possible to treat rigorously the problem of conduction in heterogeneous media for only a few simple systems. The flow of current in the steady state is given by Laplace's equation, subject to the continuity relations for potential and flux at the common boundaries between phases.

A comprehensive review of the literature published before 1962 was given by Meredith and Tobias [28]. They mainly concerned themselves with "porphyritic" dispersions, those characterized by one continuous phase in which particles of one or more distinct phases are embedded. They presented solutions for dilute suspensions of ellipsoidal particles of uniform size. The solutions are accurate for both random and ordered dispersions, when the volume fraction for the dispersed phases is under about 0.1. The basic assumption behind these solutions is that the field disturbances around the dispersed particles do not influence each other. These solutions are said to be accurate to order c, where c is the volume fraction of the particles. Although the solutions are derived for particles of uniform size, at very low values of the volume fractions of the dispersed phase, differences in particle size will not cause a noticeable difference in effective conductivities.

Bernardi [2] used one of these models, Maxwell's spherical particle model, for the matrix conductivity in the FeS electrode. She

assumed that the discrete phases were Fe and voids (filled with electrolyte) and lumped all the other electrode phases together into the continuous phase. As mentioned before, this procedure had only limited success.

Meredith and Tobias [28] also presented rigorous treatments for ordered dispersions of spheres and cylinders, as well as a large number of effective conductivity approximations.

The effective-medium approximation is a widely used method for approximating the effective conductivity of a heterogeneous system. Hahin [29] calls his version of this the "self consistent scheme" approximation method, and he states that "the basic underlying assumption is that a typical basic element of a heterogeneous medium, such as a single crystal in a polycrystal or an inclusion in a particulate composite, can be regarded as being embedded in an equivalent homogeneous medium whose properties are the unknowns to be calculated." Hashin examined systems in which a particulate phase was contained in a matrix phase. He considered a spherical inclusion that was surrounded by a shell of the matrix phase. The sphere and its shell were then embedded in the effective medium whose conductivity was to be calculated. The final result contained a parameter which was given by the ratio of the outer radius of the inclusion to that of its shell (δ). This parameter is, in general, hard to specify; therefore, Hashin admitted that the approximation does not yield any more information than effective conductivity bounds that had already existed. Hashin and Shtrikman [30] derived these bounds using variational principles.

The bounds provide the most restrictive limits possible on the effective conductivity for a statistically homogeneous and isotropic two phase composite, of arbitrary phase geometry, when the only available geometrical information is the phase volume fractions. The difference between the upper and lower bounds increases as the difference between the conductivities of the two phases increases.

Acrivos and Chang [31] recently presented a technique for estimating the effective conductivities in two-phase materials of random structure by extending, in an approximate manner, the effective continuum description of such systems. This technique involves the application of effective medium models in which the particle density function is allowed to vary locally. They applied this method to calculate the effective conductivity of a random dispersion of spheres of equal sizes to order $O(c^2)$, and their results were in excellent agreement with the exact expression given by Jeffrey [32].

Jeffrey made use of the solution to the two-sphere problem to solve for the effective conductivity to order $O(c^2)$ for a stationary, random, statistically homogeneous suspension of spherical particles in a matrix of uniform conductivity. It was assumed that a second sphere occupies all positions relative to a reference sphere with equal probability. Jeffrey compared his results with those of Hashin and calculated δ for various pure-phase conductivity ratios. It is interesting to note that δ varied over a range of only 0.22 to 0.25 as the conductivity ratio varied from 0 to ∞.

The only geometrical parameters in the effective conductivity expressions discussed above are the volume fractions of the component phases. We are now ready to consider models that use a more detailed description of the medium's micro-structure. Beran [33] studied impenetrable spherical inclusions randomly and isotropically distributed throughout a matrix. He developed a scheme for generating a whole hierarchy of bounds which includes information contained in successively higher order correlation functions characterizing the composite geometry. In order to evaluate a correlation function, the quantity that must be determined is the associated probability function. An example of these functions is the three-point probability function $S_3(r,s,t)$, which gives the probability of finding the vertices of a triangle of edge lengths r, s, and t in one phase. Researchers have continued to develop bounds on effective conductivities. Milton [34] has given an extensive review of the literature and presents rigorous bounds on the complex effective conductivity tensor of a macroscopically homogeneous d-dimensional composite constructed from n isotropic components, or phases, with scalar conductivities. Complex conductivities are appropriate for describing conduction when the applied fields oscillate but have wavelengths and attenuation lengths much larger than the composite inhomogeneities.

Corson [35] used photomicrographs of material cross sections to generate the required statistical data to evaluate the third order Beran bounds. Corson compared the resultant bounds with experimental data on effective thermal conductivity, and with the less restrictive

Hashin-Shtrikman bounds. Beran bounds are a significant improvement over the Hashin-Shtrikman bounds, with the greatest improvement occurring for low phase-thermal-conductivity ratios.

Torquato [36] used the Pade´ approximation technique to evaluate the Beran bounds and gives forth order bounds for the effective conductivity. Torquato claims that his results should accurately estimate the effective conductivity of a dispersion of fully penetrable spheres, provided that the inclusion concentration is below approximately 0.2. Torquato and Lado [37] used a model of equal-sized, impenetrable spheres randomly and isotropically distributed throughout a matrix to evaluate the third-order Beran bounds up to volume fractions near the close-packing value.

Turner [38] compared the models of Maxwell, Rayleigh, and Jeffrey with experimental results. He considered beds of solid spheres (either ion-exchange resin or non-sulphonated resin) fluidized by aqueous solutions of sodium chloride. Turner concluded the following:

> The experimental results presented here show that the Maxwell relation may, for practical purposes, be used for dispersions of spheres in a continuous medium for values of c [he calls it f] up to the packed-bed value provided that the ratio for the conductivities, α, is less than about 10. The differences between different theoretical treatments in this region are small, and would require more precise measurements for an experimental decision to be made between them. The Maxwell relation remains ade-

quate, and its simplicity is attractive.

For higher values of α, the Maxwell relation becomes less useful. For $\alpha > 100$ it can continue to be used for $c < 0.2$, say, where the results become almost independent of α. For high values of α and c, the theories are quite inadequate. These are situations which could be of practical importance, and here the results can be very sensitive to c and to the mode of formation of the dispersion.

Torquato and Lado [14] compared Turner's data with their evaluation of the Hashin-Shtrikman bounds and the third-order Beran and Milton [39] bounds. These models did not significantly improve upon the models examined by Turner when high values of c and α (*e.g.*, α=14400, c=0.6) were considered. As Torquato and Lado point out, it is not clear whether the equilibrium distribution in a fluidized bed is really a static and random distribution for a high concentration of spheres. For example, Turner suggests the possibility that comparatively low-resistance paths through "chains" of particles which happen to lie close together is more than first order, or even second-order, theoretical treatments can cope with.

Sabacky and Evans [40] provided an good illustration of this point. They measured effective conductivities for fluidized beds of copper particles in the size range of 270 μ to 385 μ. From the results they inferred that the dominant mechanism of electrical conduction was through "chains" of particles in momentary electrical contact.

At this point we need to stop and reflect upon the problem at hand. Our goal is to be develop an expression for the effective conductivity of the FeS_x electrode. The solid phases must be in contact in order to provide a path for the electrons to be carried from the current collector to the reaction sites. The electrolyte phase must also form a continuous path so that ions can be transported into the electrode. We have seen that the effective conductivity expressions whose only geometric parameters are volume fractions come from models involving a discontinuous phase dispersed in a continuous medium. It is doubtful that these expressions will be able to predict accurately the effective conductivities of the FeS_x electrodes. It is not practical to use the expressions that involve a statistical description of the medium because of the amount the information that would be required to describe the system accurately. Despite having an unconsolidated matrix phase, the electrodes considered here have some of the some complexities as the consolidated systems discussed by Merideth and Tobias [28]:

> A large number of solid-fluid systems exist in which the continuous phase is the solid, but at the same time a certain degree of continuity may also exist in the fluid phase. Sandstone, sintered metals, porous ceramic bodies, and porous carbon belong in this class of conductors. Here, as was not the case when we dealt with "unconsolidated" dispersions, we are seldom in the position of being able to characterize the mixture by simple geometric parameters. Conduction occurs through tortuous paths,

> fissures, and channels which can hardly be classified, not to speak of the possibility of a mathematical description. Because of the complexity of these systems, the behavior of their conductivity can at present be represented only be empirical equations of rather limited validity.

The possibility of contact resistance between particles is an additional complexity, which is not found in consolidated systems.

An alternate approach to dealing with these problems may be found in percolation theory. Kirkpatrick [41] studied simulations of resistor networks from which resistors were removed at random. These networks were related to the lattice models for which percolation thresholds and percolation probabilities had previously been considered. Kirkpatrick also formulated an effective medium theory for two bond percolation models. This effective medium theory accurately described the effective conductivity, except for concentrations close to the percolation threshold. Near the threshold, the effective conductivity followed a power law form,

$$\sigma^* \propto (p - p_c)^{1.5-1.6} , \tag{5-3}$$

where p is the fraction of bonds present and p_c is the threshold bond fraction. The electrical conductivity at a continuum percolation transition was found to obey the power law

$$\sigma^* \propto (p - p_c)^{1.4} \tag{5-4}$$

by Webman and Jortner [42].

5.3. Summary

An accurate expression for the effective conductivity of the solid matrix in FeS_x electrodes has not been found. A solution to this problem could be used to improve mathematical models of the Li(Alloy)/FeS_x battery system. Any general theory developed while solving this problem could have many applications because of the large number of problems involving transport in heterogeneous media.

Finally, I should like to note that it is possible that a simple expression for the effective conductivity, such as Maxwell's equation, might work if it is applied to the FeS_x electrode in the correct way. This changes the problem from one of finding an expression for the effective conductivity to one of examining the micro-structure of the medium and deciding how a simple model can be applied to the real system.

List of Symbols

A	area (cm^2)
ASR	area-specific resistance ($\Omega \cdot cm^2$)
d	one-half the distance between the positive current collector and the post centers (cm)
DOD	depth of discharge
E	energy (J)
f	see Equation 4-14
H	height of the positive current collector (cm)
I	current (A)
i	current density (A/cm^2)
L	length (cm)
N	number of electrodes
P	power (W)
Q	capacity (C)
r	radius (cm)
R	resistance (Ω)
T	thickness of bus (cm)
U	apparent-open-circuit potential (V)
V	voltage (V)
W	weight (kg)
y	height coordinate (cm)

Greek letters

α	penetration depth (cm) - see Equation 4-6
β	see Equation 4-13
δ	see Equation 3-4
γ	see Equation 4-12
ϕ	potential with respect to negative current collector (V)
ρ	density (g/cm^3)
σ	conductivity (S/cm)
θ	see Equation 4-10

Subscripts

base	excluding bus and post
bus	interconnecting bus
c	can
cut	at cut-off voltage
i	positive current collector
o	separator
pos	positive electrode
post	cell post
t	total
+	positive electrode
−	negative electrode

Superscripts

^	specific (per kg)
'	refers to bus and post combination

References

[1] E. C. Gay, R. K. Steunenberg, W. E. Miller, J. E. Battles, T. D. Kaun, F. J. Martino, J. A. Smaga, and A. A. Chilenskas, *Li-Alloy/FeS Cell Design and Analysis Report*, Argonne National Laboratory Report ANL-84-93 (July, 1985).

[2] Dawn Bernardi, *Mathematical Modeling of Lithium(Alloy)/Iron Sulfide Cells and the Electrochemical Precipitation of Nickel Hydroxide*, Dissertation, University of California, Berkeley (1986).

[3] T. D. Kaun, L. Redey, and P. A. Nelson, "Molten Salt Battery Advances," *Proceedings of the 22nd Intersociety Energy Conversion Engineering Conference*, Philadelphia, PA, pp. 1085-1090 (1987).

[4] J. R. Selman and D. Topor, "Corrosion Resistant Coatings for High-Temperature High-Sulfur-Activity Applications," *Final Report, October 1986, Lawrence Berkeley Laboratory, Technology Base Research Project.*

[5] D. R. Vissers, Z. Tomczuk, L. Redey, and J. Battles, *High Temperature Lithium Alloy/Iron Sulfide Batteries*, Chapter 10 in "Lithium: Current Applications in Science, Medicine, and Technology," Ricardo O. Bach, editor, John Wiley and Sons, Inc., New York (1985), pp 121-154.

[6] S. K. Preto, Z. Tomczuk, S. von Winbush, and M. F. Roche, "Reactions of FeS_2, CoS_2, and NiS_2 Electrodes in Molten LiCl-KCl Elec-

trolytes," *Journal of the Electrochemical Society*, 130, no. 2, pp. 264-273 (February, 1983).

[7] Thomas D. Kaun, "LiAl/FeS_2 Cell with LiCl-LiBr-KBr Electrolyte," *Journal of the Electrochemical Society*, 132, no. 12, pp. 3063-3064 (December, 1985).

[8] L. Redey and T. Kaun, report titled *Molten-Electrolyte Cell Research*, in "Technology Base Research Project for Electrochemical Energy Storage," Lawrence Berkeley Laboratory Annual Report for Fiscal Year 1985, pp. 17-19 (July, 1986).

[9] P. A. Nelson and H. Shimotake, U.S. Patent No. 4,357,398 (1982).

[10] Gary George Trost, *Applications of Porous Electrodes to Metal-Ion Removal and the Design of Battery Systems*, Dissertation, University of California, Berkeley (1983)

[11] Gary G. Trost, Victoria Edwards, and John Newman, "Electrochemical Reaction Engineering," Chapter 14 in "Chemical Reaction and Reactor Engineering," James J. Carberry and Arvind Varma, editors, Marcel Dekker, Inc., New York (1987), pp. 923-972.

[12] William H. Tiedemann and John Newman, "Mathematical Modeling of the Lead-Acid Cell," *Proceedings of the Symposium on Battery Design and Optimization* (The Electrochemical Society, volume 79-1, 1979), pp. 23-38

[13] William H. Tiedemann and John Newman, "Current and Potential Distribution in Lead-Acid Battery Plates," *Proceedings of the Symposium on Battery Design and Optimization* (The Electrochemical Society, volume 79-1, 1979), pp. 39-49.

[14] H. Gu, R. L. Galyen, and G. W. Brutchen, "An Empirical Modelling Approach to Designing a Battery," *Electrochemical Engineering Applications*, Ralph E. White, Robert F. Savinell, and Alfred Schneider, eds., AIChE Symposium Series, **83** (No. 229), pp. 92-95 (1983).

[15] Kenji Asai, Teruhiro Hatanaka, Masaharu Tsubota, Kunio Yonezu, and Koji Ando, "Design Optimization of Tall Tubular Lead/Acid Cells Based on an Analysis of the Reaction Distribution," *Journal of Power Sources*, **16**, 65 (1985).

[16] L. Redey, J. A. Smaga, J. E. Battles, and R. Guidotti, *Investigation of Primary Li-Si/FeS_2 Cells*, Argonne National Laboratory Report ANL-87-6, (April, 1987).

[17] J. Newman, S. Higuchi, and L. Redey, *Electrochemical Model (Micro)*, in Argonne National Laboratory Report ANL-80-128, pp. 67-79 (February, 1981).

[18] Thomas D. Kaun, *Development of the Lithium-Limited FeS Cell*, Argonne National Laboratory Report ANL-86-40, pp. B-101 to B-114 (April, 1986).

[19] L. Redey and D. R. Vissers, *Electrochemical Characteristics of Li-Alloy and MS_2 Electrodes*, in Argonne National Laboratory Report ANL-83-62, pp. 14-18 (September, 1983).

[20] Thomas Kaun, Personal communication (1987).

[21] L. A. Eaton, *Cell Component Development*, in Argonne National Laboratory Report ANL-79-94, pp. 31-37 (March, 1980).

[22] S. M. Zivi, H. Kacinskas, I. Pollack, A. A. Chilenskas, W. Grieve, B. L. McFarland, and S. Sudar, *Conceptual Design for Utility Load-Leveling Battery with Li/FeS Cells*, Argonne National Laboratory Report ANL-80-20 (July, 1980).

[23] E. P. Adams, "Electrical Distributions on Circular Cylinders," *Proceedings of the American Philosophical Society*, 75, 11 (1935).

[24] Z. Tomczuk, S. K. Preto, and M. F. Roche, "Reactions of FeS Electrodes in LiCl-KCl Electrolyte," *Journal of the Electrochemical Society*, 128, 760 (1981).

[25] R. Pollard, *Mathematical Modeling of the Lithium-Aluminum, Iron Sulfide Battery*, Dissertation, University of California, Berkeley (1979).

[26] John Newman and William Tiedemann, "Porous-Electrode Theory with Battery Applications," *AIChE Journal*, 21, 25 (1975).

[27] John Newman, "Modeling of Porous Electrodes in Molten-Salt Systems," *International Workshop on High-Temperature Molten Batteries*, Argonne National Laboratory, LBL-21867, August, 1986.

[28] Robert E. Meredith and Charles W. Tobias, "Conduction in Heterogeneous Systems," *Advances in Electrochemistry and Electrochemical Engineering 2*, Charles W. Tobias, editor, John Wiley and Sons, Inc., New York(1962), pp 15-47.

[29] Zvi Hashin, "Assessment of the Self Consistent Scheme Approximation: Conductivity of Particulate Composites," *Journal of Composite Materials*, 2, 284 (1968).

[30] Z. Hashin and S. Shtrikman, "A variational approach to the theory of the effective magnetic permeability of multiphase materials," *Journal of Applied Physics*, 33, 3125 (1962).

[31] Andreas Acrivos and Eric Chang, "A Model for Estimating Transport Quantities in Two-Phase Materials," *Phys. Fluids*, 29, 3 (1986).

[32] D. J. Jeffrey, "Conduction through a random suspension of spheres," *Proceedings of the Royal Society of London*, *A*, 335, 355 (1973).

[33] M. J. Beran, "Use of the Variational Approach to Determine Bounds for the Effective Permittivity of Random Media," *Nuovo Cimento*, 38, 771 (1965).

[34] G. W. Milton, "Multicomponent Composites, Electrical Networks and New Types of Continued Fraction I and II," *Communications in Mathematical Physics*, 111, 281 (1987).

[35] Peter B. Corson, "Correlation Functions for Predicting Properties of Heterogeneous Materials. I-IV," *Journal of Applied Physics*, 45, 3159 (1974).

[36] S. Torquato, "Effective Electrical Conductivity of Two-Phase Disordered Composite Media," *Journal of Applied Physics*, 58, 3790 (1985).

[37] S. Torquato and F. Lado, "Effective Properties of two-phased disordered composite media: II. Evaluation of Bounds on the Conductivity and Bulk modulus of dispersions of Impenetrable Spheres," *Physical Review B*, 33, 6428 (1986).

[38] J. C. R. Turner, "Two-Phase Conductivity: The Electrical Conductance of Liquid-Fluidized Beds of Spheres," *Chemical Engineering Science*, 31, 487 (1976).

[39] G. W. Milton, "Bounds on the Complex Permittivity of a Two-Component Composite Material," *Journal of Applied Physics*, 52, 5286 (1981).

[40] B. J. Sabacky and J. W. Evans, "The Electrical Conductivity of Fluidized Bed Electrodes-Its Significance and Some Experimental Measurements," *Metallurgical Transactions B*, 8B, 5 (1977).

[41] Scott Kirkpatrick, "Percolation and Conduction," *Reviews of Modern Physics*, 45, 574 (1973).

[42] Itshak Webman, Joshua Jortner, and Morrel H. Cohen, "Numerical Simulation of Continuous Percolation Conductivity," *Physical Review B*, 14, 14 (1976).

[43] Thomas D. Kaun, "A Stable, High-Performance Lithium(Alloy)/Iron Disulfide Cell with LiCl-LiBr-KBr Molten Electrolyte," Proceedings of the 19th Intersociety Conference, San Diego, CA, pp. 1048-1051 (1986).

Appendix A

Program PRISMATIC Code

```
      PROGRAM prismatic
c*************************************************************************
c*           This program models a LiAl/FeS prismatic cell.              *
c*           The data comes from ANL-80-128.  The cell design is         *
c*           based on ANL-79-94.                                         *
c*************************************************************************
  101 FORMAT (I4,5E12.5,2F5.3)
  102 FORMAT (X,F6.4,F11.4,2F10.7,6F10.4,F10.7)
  103 FORMAT (1H1)
  104 FORMAT (8H0QLPOST=,F5.3,5X,6HQLBUS=,F6.3)
  105 FORMAT(14H0PLATE HEIGHT=,F6.2,12H CM,  WIDTH=,F6.2,16H CM,  THICKN
     1ESS=,F6.3,18H CM,  GRID WEIGHT=,F10.4,2H G)
  106 FORMAT (9H0DEPTH OF,2X,7HCURRENT,3X,6HRESIST,4X,6HRPRIME,4X,6HENER
     1GY,8X,20HSPECIFIC POWER, W/KG,7X,6HWEIGHT/ X,9HDISCHARGE, 4X,1HA,
     28X,3HOHM, 7X,3HOHM,5X,7HW-HR/KG,5X,4HZERO,6X,4HHALF,6X,3HEND, 6X,6
     33HKG/POS)
  107 FORMAT (28X,F10.7,6F10.4)
  108 FORMAT (19H WP/RHO/THICK/AREA=,F 7.4,5X, 5HDIM1=,F 8.4,5X,5HNPOS=,
     1I3,5X,20HAREA*Y0/THICK/SGRID=,F8.4)
  109 FORMAT (9E8.4)
  110 FORMAT ( 8H RATTOP=,F6.3,2X,7HRATCTR=,F6.3)
  111 FORMAT (7H0WPMIN=,F9.4,2X,6HWNMIN=,F9.4,2X,3HWN=,F9.4,2X,5HWAMP=,
     1F9.4,2X,5HWAMN=,F9.4,2X,6HWELEC=,F9.4,2X/7H CANWT=,F9.4,2X,10HAMPH
     2R/POS=,F9.4,2X,7HTAMPHR=,F9.4)
  112 FORMAT(1X,'WBUS=',F8.4,2X,'WPOST=',F8.4,2X,'CSAB=',F8.4,2X,
     1'CSAP=',F8.4)
  113 FORMAT(1X)
  114 FORMAT (7H0WPMIN=,F9.4,2X,6HWNMIN=,F9.4,2X,3HWN=,F9.4,2X,5HWAMP=,
     1F9.4,2X,5HWAMN=,F9.4,2X,6HWELEC=,F9.4,2X/7H CANWT=,F9.4,2X,
     29HNSTRINGS=,I2,2X,10HAMPHR/POS=,F9.4,2X,7HTAMPHR=,F9.4,2X,
     37HAAMPHR=,F9.4)
  115 FORMAT (1X,'MAXIMUM ENERGY')
  116 FORMAT (1X,'MAXIMUM POWER')
  117 FORMAT (F6.4,F10.4,F10.6,F6.4,F10.4,F10.6,F6.4,F10.4,F10.6)
  118 FORMAT (1X,'COMPROMISE')
  119 format (1x,'modecc=',i2,3x,'mode=',i2,3x,'iamode=',i2,3x,
     1           'vcut= ',f6.3,' volts')
  120 format (1x,'anthick= ',f10.4,' cm',3x,
     1         'aratio= ',f10.4,3x,'awtrat= ',
     2        f10.4,3x,'adodf= ',f10.4)
      DIMENSION S1(500),S2(500),RESIST(500),OPEN(500),QFRACT(500),YI(500
     1)
```

```
      COMMON /GRID/NDATA,HEIGHT,WIDTH,WP,RESIST,RHGRID,SGRID,THICK,YI,
     1SEPEFF
      COMMON/OY/QFRACT,QMAX,OPEN,VCUT
      COMMON/EBI/EMAXE,ENERG1,ENERG2,ENERG3,WP1,WP2,WP3,IFLAGG
     1,IBISEC,PMAXP,IPFLAG
      common/andy/ awtrat,aratio
c     - descriptions of modes ......
C     MODE = 1 IS FOR NO AMPHR CONSTRAINTS, MUST READ IN THE AREA
C     MODE = 2 IS FOR A TOTAL AMPHR CONSTRAINT
C     MODE = 3 IS SAME AS MODE = 1, EXCEPT PICKING UP BITS OF DOD FOR
C     MAX POWER
C     MODE = 4 IS SAME AS MODE = 2, EXCEPT PICKING UP BITS OF DOD FOR
C     MAX POWER
C     MODECC = 1 IS TO INCLUDE MIN CC WEIGHTS ACTUALLY INTO THE CURRENT
C     COLLECTOR
C     MODECC = 0 IS WHEN YOU DON'T WANT TO DO THIS
c     iamode = 0 The thickness of the negative electrode, ANTHICK,
c                is determined by the input.  The weight of the
c                negative active material, WAMN, is calculated.
c     iamode = 1 ANTHICK is calculated so that WAMN is equal to that
c                given in the input.  WN or WNMIN is used depending
c                on MODDEC and WN.
c     iamode = 2 ANTHICK is calculated so that the value of WAMN
c                is given by the input and WN = WNMIN.
c     - initialize variables...
C     TO USE BISECTION ROUTINE, SET IBFLAG=1
C     FOR BISECTION, NOTE THAT LMODE IF STATEMENTS HAVE TO BE ADJUSTED.
      IBFLAG=0
      MOD=1
      ENERG3=0.0
      POW3=0.0
      WP3=0.0
      IFLAGG=0
      IPFLAG=0
      IBISEC=0
c     - the following values are specific to a given cell.....
      read *,npos
      read *,rhgrid
      read *,anrhgrid
      read *,sgrid
      read *,sepeff
      print 121,npos,rhgrid,anrhgrid,sgrid,sepeff
 121  format(1x,'npos= ',i3,3x,'rhgrid= ',f6.3,' g/cc',
     &         3x,'anrhgrid= ',f6.3,' g/cc',
     &          3x,'sgrid= ',f7.1,' 1/(ohm*cm)',3x,'sepeff= ',f5.3,
     &          ' ohm*sq.cm.')
      read *,rhpost
      read *,spost
      read *,rhbus
      read *,sbus
      print 122,rhpost,spost,rhbus,sbus
```

```
 122  format(1x,'rhpost= ',f6.3,' g/cc',3x,'spost= ',f7.1,' 1/(ohm*cm)',
     &          ' rhbus= ',f6.3,' g/cc',3x,'sbus= ',f7.1,' 1/(ohm*cm)')
      read *,y0
      read *,u0
      read *,qls
      read *,epsp
      read *,timed
      print 123,y0,u0,qls,epsp,timed
 123  format(1x,'y0= ',f10.5,' 1/(ohm*sq.cm.)',3x,'u0= ',f7.4,' V',
     &          3x,'qls= ',f5.3,' cm',3x,'epsp= ',f4.2,3x,'timed= ',
     &          f7.1,' sec.')
      read *,aload
      read *,anload
      read *,aspcap
      read *,anspcap
      print 124,aload,anload,aspcap,anspcap
 124  format(1x,'aload= ',f7.4,' g/cc',3x,'anload= ',f7.4,' g/cc',
     &       3x,'aspcap= ',f7.2,' C/g',3x,'anspcap= ',f7.2,' C/g')
    5 CONTINUE
c     - input and echoprint....
      read *, modecc, mode, iamode, aratio,vcut
      aconv = anspcap/aspcap
      if (iamode .eq. 1  .or.  iamode .eq. 2) then
         awtrat = aratio/aconv
         adodf = aratio
      endif
      READ *, NDATA,HEIGHT,WIDTH
      READ *, THICK,anthick
      READ *, WP,wn,RATTOP,RATCTR
      print *,'************************************************************'
      if (mode .eq. 2) then
         read *, totcap, junk
         print 113
         print 113
         print *,'totcap= ',totcap,' A-hrs'
      else
         read *, ajunk, junk
         print 113
         print 113
      endif
      IF(NDATA.EQ.0) STOP
      q0 = aspcap*aload
      print 119,modecc,mode,iamode,vcut
      print *,'ndata = ',ndata
   28 CONTINUE
      PRINT 103
      READ *, RAT1,RAT2
      ENERG3=0.0
      POW3=0.0
      WP3=0.0
      IFLAGG=0
```

```
      IPFLAG=0
      IBISEC=0
   83 CONTINUE
      QLPOST=0.001
      QLBUS=0.001
      IF (MODE .EQ. 4) MOD=1
   84 CONTINUE
      IF ((MODE .EQ. 1) .OR. (MODE .EQ. 3)) GO TO 13
      DOD=1.
      NSTRNG=1
      CAP = TOTCAP/FLOAT(NSTRNG)
   12 AREA= CAP*3600.0/(Q0*DOD*THICK*FLOAT(NPOS)) + WP/RHGRID/THICK
      HEIGHT=SQRT(AREA)
      WIDTH=HEIGHT
      DODOLD=DOD
   13 CONTINUE
c     - calculate quantities required to describe the cell
c       some calculations are specific to the cell design
      WPMIN=2.0*(HEIGHT*WIDTH-0.45*(HEIGHT-0.3)*(WIDTH-0.3)+2.0*THICK*
     1(HEIGHT+WIDTH))*0.010*2.54*RHGRID
      if (modecc.eq.1 .and. wpmin.gt.wp) then
         wp = wpmin
         if (mode .eq. 4) then
            print *, 'AAM: ************** error 300'
         endif
      endif
      wamp = aload*thick*(height*width-wp/rhgrid/thick)
      if (iamode .eq. 0) then
         atemp = float(npos-1)
         WNmin=(2.0*atemp*(HEIGHT*WIDTH-0.45*(HEIGHT-0.3)*(WIDTH-0.3)
     1   +2.0*anthick*(HEIGHT+WIDTH)) + 2.0*anthick*(height+width)
     2 +4.0*height*width -2.0*0.45*(width-0.3)*(height-0.3))*0.010*2.54*
     3   anRHGRID/float(npos)
         if (modecc.eq.1 .and. wnmin.gt.wn) wn=wnmin
      else
         wamn = wamp*awtrat
         anthick=wamn/anload/height/width + 2.0*(0.01*2.54)
         iacount = 0
   86    continue
           iacount = iacount + 1
           atemp = float(npos-1)
         WNmin=(2.0*atemp*(HEIGHT*WIDTH-0.45*(HEIGHT-0.3)*(WIDTH-0.3)
     1   +2.0*anthick*(HEIGHT+WIDTH)) + 2.0*anthick*(height+width)
     2 +4.0*height*width -2.0*0.45*(width-0.3)*(height-0.3))*0.010*2.54*
     3   anRHGRID/float(npos)
           anthick = (awtrat*wamp/anload + wnmin/anrhgrid)/height/width
           atest1=anload*anthick*(height*width-wnmin/anrhgrid/anthick)
           atest2 = abs(atest1-wamn)
           if (iacount .gt. 50) then
              print *,'AAM:************** error 100'
           endif
```

```
            if (atest2 .gt. 0.01) go to 86
            if (iamode .eq. 2) then
               wn = wnmin
            else
               if (modecc.eq.1 .and. wnmin.gt.wn) wn=wnmin
               anthick = anthick + (wn-wnmin)/anrhgrid/height/width
            endif
         endif
         wamn = anload*anthick * (height*width - wn/anrhgrid/anthick)
         awtrat = wamn/wamp
c        - use Trost's value for electrolyte density; density = 1.6477g/cc
         welec=(0.6*wamn + 0.4*wamp + 2.0*qls*1.6477*(height*width))*1.1
         canthk = (thick+anthick+2.0*qls)*float(npos)
         CANWT=(CANTHK*(2.0*(HEIGHT+1.5)+2.0*(WIDTH+0.4))+(HEIGHT+1.5)*
        1(WIDTH+0.4)*2.0)*7.86*0.061
         AMPHR=Q0*(HEIGHT*WIDTH*THICK-WP/RHGRID)/3600.0
         TAMPHR=AMPHR*FLOAT(NPOS)
         QMAX=Q0*THICK/2.0
         FEEDWT=50.0
         BUSWT=20.0
         WEIGHT= (CANWT+FEEDWT+BUSWT)/FLOAT(NPOS)+WAMP+WAMN+WP+WN+WELEC
         BASEWT=WEIGHT/1000.0-0.02/FLOAT(NPOS)
         if (iamode .eq. 0) then
            awtrat = wamn/wamp
            aratio = awtrat*aconv
            adodf = aratio
         endif
c        - begin calculations .....
         CALL GRID
      27 CONTINUE
         DIM1=HEIGHT*WIDTH*SQRT(RHGRID*Y0/WP/SGRID)
         FRACWT=WP/RHGRID/THICK/HEIGHT/WIDTH
         DIMGT= FRACWT*DIM1**2
         IF ((MODE .EQ. 2) .OR. (MODE .EQ. 4)) GO TO 15
         PRINT 113
         PRINT 113
         PRINT 105, HEIGHT, WIDTH,THICK,WP
         PRINT 110 , RATTOP,RATCTR
         PRINT 111, WPMIN,WNMIN,WN,WAMP,WAMN,WELEC,CANWT,AMPHR,TAMPHR
         PRINT 108, FRACWT,DIM1,NPOS,DIMGT
         print 120, anthick, aratio, awtrat, adodf
         PRINT 113
         PRINT 106
      15 CONTINUE
         S1(1)=0.0
         S2(1)=0.0
         E2=0.0
         E4=0.0
       1 DELTA=0.004*(QLBUS*SQRT(RHBUS/SBUS)+QLPOST*SQRT(RHPOST/SPOST))**2
         IF (QLPOST .LT. 0.5) LMODE=0
         IF ((QLPOST .GT. 0.5) .AND. (QLPOST .LT. 4.)) LMODE=2
```

```
      IF (QLPOST .GT. 4.) LMODE=5
      IF ((MODE .EQ. 2) .OR. (MODE .EQ. 4)) GO TO 16
      PRINT 113
      PRINT 104, QLPOST,QLBUS
   16 IF ((MODE .EQ. 4) .AND. (MOD .GT. 1)) GO TO 24
      DO 2 I=2,NDATA
      DOD=1.0-QFRACT(I)
      DODD=(OPEN(I)-OPEN(I-1))/(QFRACT(I-1)-QFRACT(I))
      DRDD=(RESIST(I)-RESIST(I-1))/(QFRACT(I-1)-QFRACT(I))
      CUR=DOD/TIMED*Q0*THICK*(HEIGHT*WIDTH-WP/RHGRID/THICK)
      V=OPEN(I)-RESIST(I)*CUR
      RPRIME=(V-VCUT)/CUR
      IF(QLPOST.GT.0.5)GO TO 7
      E3=E4
      E4=OPEN(I)-VCUT-RESIST(I)*CUR
      S1(I)=S1(I-1)+(OPEN(I)+OPEN(I-1))/2.*(QFRACT(I-1)-QFRACT(I))
      S2(I)=S2(I-1)+(RESIST(I)+RESIST(I-1))/2.*(QFRACT(I-1)-QFRACT(I))
      IF(E4.GT.0.0) GO TO 2
      F2=-E4/(E3-E4)
      GO TO 8
    7 E1=E2
      F2=0.0
c     IF(DOD.LT.0.5) GO TO 2
c     IF(DOD.LT.0.64 .AND. FRAC WT.GT.0.08) GO TO 2
      IF(DOD.GT.DODMAX) F2=(DOD-DODMAX)/(QFRACT(I-1)-QFRACT(I))
      F3=F2
      DO 11 K=1,3
      IF(K.EQ.2) E3=E2
      DOD=1.-QFRACT(I)-F2*(QFRACT(I-1)-QFRACT(I))
      CUR=DOD/TIMED*Q0*THICK*(HEIGHT*WIDTH-WP/RHGRID/THICK)
      RES=RESIST(I)+F2*(RESIST(I-1)-RESIST(I))
      OP=OPEN(I)+F2*(OPEN(I-1)-OPEN(I))
      RPRIME=(OP-VCUT)/CUR-RES
      SUM1=S1(I)+F2*(S1(I-1)-S1(I))
      SUM2=S2(I)+F2*(S2(I-1)-S2(I))
      E2=(BASEWT*RPRIME+DELTA)*RPRIME*CUR*(VCUT+CUR*RES-DOD*DODD+DOD*CUR
     1*DRDD-CUR/DOD*SUM2)-(SUM1/DOD-CUR*RPRIME-CUR/DOD*SUM2)*DELTA*
     2(OP-VCUT-DOD*DODD+DOD*CUR*DRDD)
      IF(E2.GT.0.0 .AND. K.EQ.1) GO TO 2
      DF=-E2/(E1-E2)*(1.0-F2)
      IF(K.EQ.1) GO TO 11
      C=E2*(1.0-F2)*(F2-F3)
      A=-E2
      IF(K.GT.2) A=A+(E1*(F2-F3)+E3*(1.-F2))/(1.-F3)
      B=(E1-E2)*(F2-F3)-A*(1.-F2)
      IF(B**2.LT.4.*A*C) GO TO 11
      DF=-2.0*C/(B+SQRT(B**2-4.*A*C))
   11 F2=F2+DF
    8 SUM1=S1(I)+F2*(S1(I-1)-S1(I))
      SUM2=S2(I)+F2*(S2(I-1)-S2(I))
      OP=OPEN(I)+F2*(OPEN(I-1)-OPEN(I))
```

```
   RES=RESIST(I)+F2*(RESIST(I-1)-RESIST(I))
   DOD=1.-QFRACT(I)-F2*(QFRACT(I-1)-QFRACT(I))
   IF(QLPOST.LT.0.5) DODMAX=DOD
   HALF=1.0-DOD/2.
   IF ((MODE .EQ. 1) .OR. (MODE .EQ. 3)) GO TO 14
   IF (ABS(DOD-DODOLD) .GT. 0.000001) GO TO 12
23 AAMPHR=DOD*TAMPHR
   PRINT 113
   PRINT 113
   PRINT 105, HEIGHT, WIDTH,THICK,WP
   PRINT 110, RATTOP,RATCTR
   PRINT 114, WPMIN,WNMIN,WN,WAMP,WAMN,WELEC,CANWT,NSTRNG,AMPHR,
  1TAMPHR,AAMPHR
   PRINT 108, FRACWT,DIM1,NPOS,DIMGT
   print 120, anthick, aratio, awtrat, adodf
   PRINT 113
   PRINT 106
   PRINT 104, QLPOST,QLBUS
   IF (QLPOST .LT. 0.5) GO TO 14
   IF ((MODE .EQ. 4) .AND. (MOD .EQ. 1)) PRINT 115
   IF ((MODE .EQ. 4) .AND. (MOD .EQ. 2)) PRINT 116
   IF ((MODE .EQ. 4) .AND. (MOD .EQ. 3)) PRINT 118
14 IF ((MODE .EQ. 4) .AND. (MOD .GT. 1)) GO TO 9
   CUR=DOD/TIMED*Q0*THICK*(HEIGHT*WIDTH-WP/RHGRID/THICK)
   RPRIME=(OP-VCUT)/CUR-RES
   RMAX=(SUM1/CUR-SUM2)/DOD
   RMAX=RMAX/(1.0+SQRT(1.0+BASEWT/DELTA*RMAX))
   MOD=1
   IF(RMAX.LT.RPRIME) RPRIME=RMAX
   R3=RMAX
   WEIGHT=BASEWT+DELTA/RPRIME
   DO 3 K=2,NDATA
 3 IF(QFRACT(K).LT.HALF) GO TO 4
   K=NDATA
 4 L=K
   F=(HALF-QFRACT(L-1))/(QFRACT(L)-QFRACT(L-1))
   RHALF= 1.0/(1.0/RESIST(L-1)+F*(1.0/RESIST(L)-1.0/RESIST(L-1)))
   OHALF=OPEN(L-1)+F*(OPEN(L)-OPEN(L-1))
 9 PNOW=OP**2/4.0/(RES+RPRIME)/WEIGHT
   P0=OPEN(1)**2/4.0/(RESIST(1)+RPRIME)/WEIGHT
   PHALF=OHALF**2/4.0/(RHALF+RPRIME)/WEIGHT
   VV=OP-CUR*RES-CUR*RPRIME
   ENERGY=Q0*(HEIGHT*WIDTH*THICK-WP/RHGRID)/WEIGHT*(SUM1-DOD*CUR*RPRI
  1ME-CUR*SUM2)/3600.0
   WPRIME=DELTA/RPRIME*1000.*FLOAT(NPOS)
   XX=QLPOST/QLBUS*SQRT(SBUS*RHPOST/RHBUS/SPOST)
   WBUS=WPRIME/(1.+XX)/FLOAT(NPOS)
   WPOST=WBUS*XX*FLOAT(NPOS)
   CSAB=WBUS/RHBUS/(2.*QLBUS)
   CSAP=WPOST/RHPOST/(2.*QLPOST)
   RCUT=(OP-VCUT)/CUR-RES
```

```
      IF(MOD.GT.1) GO TO 10
      DODE=DOD
      IF (IBFLAG .EQ. 0) GO TO 72
C     FROM HERE TO STATEMENT LABEL 72 IS FOR ENERGY BISECTION
      IF (LMODE .EQ. 0) GO TO 72
C     IF (LMODE .EQ. 2) GO TO 72
      IF (LMODE .EQ. 5) GO TO 72
      IF (IFLAGG .EQ. 1) GO TO 72
      IF (IFLAGG .EQ. 3) GO TO 72
      IF (ENERG3 .LT. 0.001) GO TO 76
      GO TO 77
   76 ENERG3=ENERGY
      GO TO 70
   77 IF (ENERGY .GE. ENERG3) GO TO 70
      GO TO 71
   70 ENERG1=ENERG3
      WP1=WP3
      ENERG3=ENERGY
      WP3=WP
      GO TO 72
   71 ENERG2=ENERGY
      WP2=WP
      IFLAGG=1
      IBISEC=0
      WPS=WP
   72 CONTINUE
      EMAXE=ENERGY
c     - check to be sure that we have not exceeded the neg. capacity
      if (dod .gt. adodf) then
         print *, 'AAM: ********************** warning 200'
      endif
      PRINT 102, DOD,CUR,RES,RPRIME,ENERGY,P0,PHALF,PNOW,WEIGHT,VV,RCUT
      PRINT 112, WBUS,WPOST,CSAB,CSAP
      RMAX=SQRT(RHALF*DELTA/BASEWT)
      IF((RMAX.GT.RPRIME) .AND. (QLPOST .GT. 0.5)) go to 6
      RPRIME=RMAX
      WEIGHT=BASEWT+DELTA/RPRIME
      R4=RMAX
      MOD=2
      IF (QLPOST .LT. 0.5) GO TO 9
      IF ((MODE .EQ. 1) .OR. (MODE .EQ. 2)) GO TO 9
   24 KI = I-3
      E2=100.
      DO 18 J=KI,NDATA
      E1=E2
      F2=0.
      F3=F2
      DO 19 K=1,4
      IF(K.EQ.2) E3=E2
      DOD=1.-QFRACT(J)-F2*(QFRACT(J-1)-QFRACT(J))
      CUR=DOD/TIMED*Q0*THICK*(HEIGHT*WIDTH-WP/RHGRID/THICK)
```

```
      RES=RESIST(J)+F2*(RESIST(J-1)-RESIST(J))
      OP=OPEN(J)+F2*(OPEN(J-1)-OPEN(J))
      SUM1=S1(J)+F2*(S1(J-1)-S1(J))
      SUM2=S2(J)+F2*(S2(J-1)-S2(J))
      HALF=1.0-DOD/2.0
      DO 20 KK=2,NDATA
   20 IF(QFRACT(KK).LT.HALF) GO TO 21
      KK=NDATA
   21 L=KK
      F=(HALF-QFRACT(L-1))/(QFRACT(L)-QFRACT(L-1))
      RHALF= 1.0/(1.0/RESIST(L-1)+F*(1.0/RESIST(L)-1.0/RESIST(L-1)))
      OHALF=OPEN(L-1)+F*(OPEN(L)-OPEN(L-1))
      RMAX=SQRT(RHALF*DELTA/BASEWT)
      RPRIME=RMAX
      WEIGHT=BASEWT+DELTA/RPRIME
      IF (MOD .EQ. 2) R4=RMAX
      IF (MOD .NE. 3) GO TO 25
      C=OHALF**2*3600.0/4.0/Q0/(HEIGHT*WIDTH*THICK-WP/RHGRID)/RAT
      A=DOD*CUR
      B=A*RHALF-SUM1+CUR*SUM2
      C=C-RHALF*(SUM1-CUR*SUM2)
      IF(B**2.LT.4.0*A*C) GO TO 6
      RPRIME=(-B-SQRT(B**2-4.*A*C))/2./A
      IF(RPRIME.LT.0.0) RPRIME=(-B+SQRT(B**2-4.*A*C))/2./A
C     IF(RPRIME.LE.0.0) GO TO 6
      WEIGHT=BASEWT+DELTA/RPRIME
C     IF(RPRIME.GT.R3 .OR. RPRIME.LT.R4)GO TO 6
   25 E2=OP-RES*CUR-RPRIME*CUR-VCUT
      IF (E2 .GT. 0.0 .AND. K .EQ. 1) GO TO 18
      DF=-E2/(E1-E2)*(1.0-F2)
      IF(K.EQ.1) GO TO 19
      C=E2*(1.0-F2)*(F2-F3)
      A=-E2
      IF(K.GT.2) A=A+(E1*(F2-F3)+E3*(1.-F2))/(1.-F3)
      B=(E1-E2)*(F2-F3)-A*(1.-F2)
      IF(B**2.LT.4.*A*C) GO TO 19
      DF=-2.0*C/(B+SQRT(B**2-4.*A*C))
   19 F2=F2+DF
      IF (MODE .EQ. 4) GO TO 26
C     IF(RPRIME.GT.R3 .OR. RPRIME.LT.R4)GO TO 6
      IF (MODE .EQ. 3) GO TO 9
   26 IF ((MODE .EQ. 4) .AND. (ABS(DODOLD-DOD) .GT. 0.0001)) GO TO 12
      IF(RPRIME.GT.R3 .OR. RPRIME.LT.R4)GO TO 6
      GO TO 23
   18 CONTINUE
   10 CONTINUE
      IF (IBFLAG .EQ. 0) GO TO 80
C     FROM HERE TO STATEMENT LABEL 80 IS FOR POWER BISECTION
      IF (MOD .EQ. 3) GO TO 80
      IF (IFLAGG .EQ. 1) GO TO 73
      IF (LMODE .EQ. 0) GO TO 73
```

```
C     IF (LMODE .EQ. 2) GO TO 73
      IF (LMODE .EQ. 5) GO TO 73
      IF (IPFLAG .EQ. 1) GO TO 73
      IF (IPFLAG .EQ. 3) GO TO 73
      IF (POW3 .LT. 0.001) GO TO 78
      GO TO 79
   78 POW3=PHALF
      GO TO 74
   79 IF (PHALF .GE. POW3) GO TO 74
      GO TO 75
   74 POW1=POW3
      WPP1=WPP3
      POW3=PHALF
      WPP3=WP
      GO TO 73
   75 POW2=PHALF
      WP2=WP
      IPFLAG=1
      IBISEC=0
      WP1=WPP1
      WP3=WPP3
      ENERG1=POW1
      ENERG2=POW2
      ENERG3=POW3
      WPS=WP
   73 CONTINUE
      PMAXP=PHALF
   80 CONTINUE
c     - check to be sure that we have not exceeded the neg. capacity
      if (dod .gt. adodf) then
         print *, 'AAM: ********************** warning 200'
      endif
      PRINT 102, DOD,CUR,RES,RPRIME,ENERGY,PO,PHALF,PNOW,WEIGHT,VV,RCUT
      PRINT 112, WBUS,WPOST,CSAB,CSAP
      IF(MOD.EQ.3)GOTO 6
      RAT=RAT1
      IF(QLPOST.GT.3.0) RAT=RAT2
      IF(QLPOST.LT.0.5) GO TO 6
      IF(RAT.EQ.0.0) GO TO 6
      MOD=3
      IF (MODE .EQ. 3) GO TO 24
      C=OHALF**2*3600.0/4.0/QO/(HEIGHT*WIDTH*THICK-WP/RHGRID)/RAT
      A=DOD*CUR
      B=A*RHALF-SUM1+CUR*SUM2
      C=C-RHALF*(SUM1-CUR*SUM2)
      IF(B**2.LT.4.0*A*C) go to 6
      RPRIME=(-B-SQRT(B**2-4.*A*C))/2./A
      IF(RPRIME.LT.0.0) RPRIME=(-B+SQRT(B**2-4.*A*C))/2./A
      IF(RPRIME.LE.0.0) go to 6
      WEIGHT=BASEWT+DELTA/RPRIME
      IF(RPRIME.GT.R3 .OR. RPRIME.LT.R4)GO TO 6
```

```
      MOD=3
      IF ((MODE .EQ. 1) .OR. (MODE .EQ. 2))   GO TO 9
      IF (MODE .EQ. 4) DOD=DODE
      IF (MODE .EQ. 4) GO TO 24
    2 CONTINUE
    6 CONTINUE
C     IF ((IFLAGG .EQ. 1) .AND. (LMODE .EQ. 0)) CALL EBISEC
C     IF ((IFLAGG .EQ. 1) .AND. (LMODE .EQ. 0)) GO TO 83
      IF ((IFLAGG .EQ. 1) .AND. (LMODE .EQ. 2)) CALL EBISEC
      IF ((IFLAGG .EQ. 1) .AND. (LMODE .EQ. 2)) GO TO 83
C     IF ((IFLAGG .EQ. 1) .AND. (LMODE .EQ. 5)) CALL EBISEC
C     IF ((IFLAGG .EQ. 1) .AND. (LMODE .EQ. 5)) GO TO 83
C     IF ((IPFLAG .EQ. 1) .AND. (LMODE .EQ. 0)) CALL EBISEC
C     IF ((IPFLAG .EQ. 1) .AND. (LMODE .EQ. 0)) GO TO 83
      IF ((IPFLAG .EQ. 1) .AND. (LMODE .EQ. 2)) CALL EBISEC
      IF ((IPFLAG .EQ. 1) .AND. (LMODE .EQ. 2)) GO TO 83
C     IF ((IPFLAG .EQ. 1) .AND. (LMODE .EQ. 5)) CALL EBISEC
C     IF ((IPFLAG .EQ. 1) .AND. (LMODE .EQ. 5)) GO TO 83
      MOD = 1
      IF(QLPOST.GT.3.0) GO TO 5
      IF(QLPOST.GT.0.5) qlpost=5.0
      IF(QLPOST.LT.0.5) QLPOST=2.0
      QLBUS=1.0
      IF ((MODE .EQ. 1) .OR. (MODE .EQ. 3)) GO TO 1
      IF ((MODE .EQ. 2) .OR. (MODE .EQ. 4)) GO TO 12
      END
c*************************************************************************
c*    This subroutine calculates the overall electrode resistance      *
c*    using the plot of dimensionless plate conductance versus         *
c*    dimensionless plate area presented in Figure 4-7 of              *
c*    Gary Trost's thesis.                                             *
c*************************************************************************
      SUBROUTINE GRID
  101 FORMAT(1X,25HX IS BEYOND INTERPOLATION,3X,3HX= ,F6.4)
      DIMENSION RESIST(500),YI(500)
      COMMON /GRID/NDATA,HEIGHT,WIDTH,WP,RESIST,RHGRID,SGRID,THICK,YI,
     1SEPEFF
      COMMON/F/X
      common/andy/awtrat,aratio
      JFLAG=0
      DO 1 I=1,NDATA
      CALL OY (Y,I,JFLAG)
      YI(I)=Y
      XX=(1.-Y*SEPEFF)/(1.-WP/RHGRID/THICK/HEIGHT/WIDTH) + Y*SEPEFF
      X1=HEIGHT*WIDTH*SQRT(RHGRID*Y/WP/SGRID)*SQRT(1./XX)
      X=0.8*X1**2/(1.+0.8*X1**2)
C     IF(X.GT.1.4) PRINT 101,X
C     IF(X.LT.0.4) PRINT 101,X
      CALL FUNC (F)
      RESIST(I)=XX/(F*2.*Y*HEIGHT*WIDTH)
    1 IF (JFLAG.EQ.1) return
```

```
      RETURN
      END
c*********************************************************************
c*    This subroutine calculates the open-circuit potential and      *
c*    the area specific conductance of the active material in the    *
c*    cell.                                                          *
c*********************************************************************
      SUBROUTINE OY (Y,I,JFLAG)
      DIMENSION QFRACT(500),OPEN(500)
      COMMON/OY/QFRACT,QMAX,OPEN,VCUT
      COMMON/GRID/NDATA
      common/andy/awtrat,aratio
      QFRACT(I)=1.-(FLOAT(I-1)/FLOAT(NDATA-1))
      xpdod = (1.0 - qfract(i))*100.0
      xndod = xpdod/aratio
      call xpos(xpdod,xposu,xpasr)
      call xneg(xndod,xnegu,xnasr)
      y = 1.0/(xpasr+xnasr)
      open(i) = xposu - xnegu
      IF (OPEN(I).LT.VCUT) JFLAG=1
      RETURN
      END
c*********************************************************************
c*    This subroutine calculates the open-circuit potential and the  *
c*    area-specific resistance of the positive active material.      *
c*********************************************************************
      subroutine xpos(xpdod,xposu,xpasr)
c     - positive U and ASR values for Trost's  cell
      if (xpdod .ge. 100.0) then
         print *,'AAM: ************************* subroutine xpos error'
         stop
      endif
c     - positive apparent open-circuit potential values ...
      qmax = 806.3
      q = qmax * (xpdod/100.0)
      xposu = 1.364 - 1.08e-4*q + 0.12498*alog(1.0-(q/qmax)**4)
c     - positive ASR values ...
      xpasr = 0.480 + 5.4e-4*q - 1.12486*alog(1.0-(q/qmax)**4)
      return
      end
c*********************************************************************
c*    This subroutine calculates the apparent open-circuit potential *
c*    and the area-specific resistance of the negative active        *
c*    material.                                                      *
c*********************************************************************
      subroutine xneg(xndod,xnegu,xnasr)
c     - negative apparent open-circuit potential  and positive ASR
c       curves for Kaun's cell.
      if (xndod .ge. 85.0) then
         print *,'AAM: ******************** error 250'
         stop
```

```
      endif
      q = 806.3 * (xndod/100.0) * 1.301
      xnegu = 0.017 + 3.6e-5*q - 0.10*alog(1.0-(xndod/85.0)**5)
      xnasr = 0.133 + 0.3042e-2*xndod - 0.15*alog(1.0-(xndod/85.0)**5)
      return
      end
c*************************************************************************
c*    This subroutine gives the equation for the curve found in       *
c*    Figure 4-7 of Gary Trost's thesis.                              *
c*************************************************************************
      SUBROUTINE FUNC (F)
      COMMON/F/X
      IF (X.LE.0.3986) F=1.00917*EXP(-1.68089*X)
      IF (X.GT.0.3986) F=-0.85866*X + 0.85866
      IF (F.GT.1.0) F=1.0
      RETURN
      END
c*************************************************************************
c*    I did not use subroutine EBISEC.                                *
c*************************************************************************
      subroutine ebisec
      return
      end
```

Sample Input for Program PRISMATIC

```
1                              npos
7.86                            rhgrid
7.86                           anrhgrid
19000.0                          sgrid
0.141                            sepeff
7.86                            rhpost
19000.0                        spost
7.86                             rhbus
19000.0                         sbus
1.63132                         y0
1.34                         u0
0.16                            qls
0.5                             doesn't matter
14400.0                         timed
2.296023                        aload
1.1182                           anload
2195.1                        aspcap
3126.0                           anspcap
1 2 1  1.25    0.90      modecc, mode, iamode, aratio, vcut
200   0.4564325 0.4563498   ndata, height, width
0.35  0.11                    thick, anthick
0.001      0.001   0.000 0.000  wp, wn, rattop, ratctr
30.0   2                      TOTCAP and junk
1.86  1.65                     rat1 and rat2
0 0 0 0.0 0.0                  flag for termination
0 0.0 0.0 0.0 0.0 0.0 0.0 0.0 0.0 0.0
0.0 0
0.0 0.0
```

List of Variables from Program PRISMATIC

adodf	DOD at which the negative capacity is exhausted
aload	loading density of the positive (g/cm^3)
amphr	capacity of one positive electrode (A-hr)
anload	loading density of the negative (g/cm^3)
anrhgrid	density of the negative grid material (g/cm^3)
anspcap	specific capacity of negative active material (C/g)
anthick	thickness of the negative electrode (cm)
aratio	ratio of negative to positive capacity
area	separator area (cm^2)
aspcap	specific capacity of positive active material (C/g)
awtrat	ratio of weights of negative to positive active materials
basewt	fraction of battery weight, excluding the bus and post weights, associated with one positive electrode (kg)
buswt	weight of bus (g)
canthk	total width of container (cm)
canwt	total weight of container (g)
cap	delivered capacity of 1 string (A-hr)
csab	cross-sectional area of the bus (cm^2)
csap	cross-sectional area of the post (cm^2)
cur	current (A)
delta	(rprime · wprime)/1000 (Ω-kg)
dod	fractional depth of discharge of the positive active material

dodd	derivative of the apparent open-circuit potential (open) with respect to dod
dodmax	depth of discharged reached with no bus or post resistance
drdd	derivative of resist with respect to dod
epsp	porosity of separator
feedwt	feedthrough weight (g)
fracwt	grid weight fraction in positive electrode
height	height of electrode (cm)
iacount	counter for loop iterations
iamode	flag - see code
mod	flag, =1 for maximum energy, =2 for maximum power, =3 for compromise design
mode	flag - see code
modecc	current collector flag - see code
ndata	number of integration intervals
npos	number of positive electrodes per cell
nstrng	number of parallel strings of cells
ohalf	apparent open-circuit potential halfway through discharge (V)
op	apparent open-circuit potential at the end of discharge (V)
open	array of apparent open-circuit potentials (V)
p0	maximum specific power when DOD=0 (W/kg)
phalf	maximum specific power halfway through discharge (W/kg)
pnow	maximum specific power at end of discharge (W/kg)
qfract	array of fractional state of charge values
qlbus	length of bus (cm)
qlpost	length of post (cm)

qls	separator length (cm)
qmax	loading of half of positive electrode (C/cm^2)
rat1	ratio of maximum specific power to maximum specific energy for a 2 cm post length
rat2	ratio of maximum specific power to maximum specific energy for a 5 cm post length
rcut	resistance of bus and post combination at end of discharge (Ω)
res	sum of electrochemical and grid resistances at the end of discharge (Ω)
resist	array containing the sum of the electrochemical and grid resistances (Ω)
rhalf	sum of electrochemical and grid resistances halfway through discharge (Ω)
rhbus	density of bus (g/cm^3)
rhgrid	density of positive current collector grid (g/cm^3)
rhpost	density of post (g/cm^3)
rprime	bus and post resistance (Ω)
s1	integral of open-circuit potentials
s2	integral of resistances
sbus	conductivity of the bus material (Ω^{-1}-cm^{-1})
sepeff	separator resistance ($\Omega \cdot cm^2$)
sgrid	conductivity of the grid material (Ω^{-1}-cm^{-1})
spost	conductivity of the post material (Ω^{-1}-cm^{-1})
tamphr	total capacity of cell (A-hr)
thick	thickness of the positive electrode (cm)
timed	time of discharge (sec)
totcap	total delivered capacity desired (mode=2 or 4) (A-hr)

u0	initial apparent open-circuit voltage (V)
V	closed-circuit voltage (V)
vcut	cutoff voltage (V)
wamn	weight of active material in the negative electrode (g)
wamp	weight of active material in the positive electrode (g)
wbus	weight of the bus (g)
weight	basewt plus associated bus and post weights (kg)
welec	weight of electrolyte associated with one positive electrode (g)
width	width of the current collector grid (cm)
wn	weight of the negative current collector (g)
wnmin	minimum weight of the negative current collector required to support the active materials (g)
wp	weight of the positive current collector (g)
wpmin	minimum weight of the positive current collector required to support the active materials (g)
wpost	weight of the post (g)
wprime	weight of the bus and post combination (g)
xnasr	area specific resistance of the negative ($\Omega \cdot cm^2$)
xndod	discharged fraction of negative capacity
xnegu	apparent open-circuit potential of the negative (V)
xpasr	area specific resistance of the positive ($\Omega \cdot cm^2$)
xpdod	discharged fraction of positive capacity
xposu	apparent open-circuit potential of the positive (V)
y0	initial value of electrochemical conductance ($\Omega^{-1} \cdot cm^{-2}$)
yi	array of values of electrochemical conductance ($\Omega^{-1} \cdot cm^{-2}$)

Appendix B

Program CYLINDER Code

```
      program cylinder
c     ************************************************************************
c     *  program cylinder makes specific energy and power calculations *
c     *     for a cylindrical cell geometry.  The data used is from    *
c     *     Kaun's LiAl/U.P. FeS2 cell.                                *
c     ************************************************************************
      dimension s1(100),s2(100),resist(100),open(100),qfract(100),
     &          yi(100)
      COMMON /collect/NDATA,rpcc,rsep,rpos,tsep,spcc,hi,RESIST,YI
      common /andy/ awtrat,aratio
      COMMON/OY/QFRACT,QMAX,OPEN,VCUT
c
c     - input data....
c
c     - MODE makes no difference
c     - if IAMODE=0 then the amount of negative active material
c       will be calculated based on the radius of the cell
c       if IAMODE=1 then the amount of negative active material
c       will be calculated using ARATIO and the radius of
c       the cell, RCAN, will be adjusted accordingly
c     - aratio = ratio of cap. neg./ cap. pos. based on full reactions
      read *,aratio,vcut
c     - aload & anload units are g/cu.cm. for pos and neg respectively
c       aspcap & anspcap are specific capacities of the pos and neg
c        based on full reactions, units are coulombs/gram.
      read *,aspcap,anspcap
      read *,ndata
      read *,height,rcan
      read *,rpcc
      read *,tpos,tsep,tncc,tcan
c     - units of dpos are g.pos./cc.electrode
c     - units of dneg are g.neg./cc.electrode
c     - units of dsep are g.total/cc.separator
      read *,dpcc,dpos,dsep,dncc,dneg,dcan,dbus,dpost
      read *,spcc,sbus,spost
      read *,rat1,rat2
      read *,npos
      read *,sepeff
      read *,y0,u0
      read *,timed
      read *,feedwt
      read *,tamphr
```

```
c     - pcc,pos,sep,ncc => apply to individual pos. electrodes
c       can,neg => apply to the whole cell
c       dpos,dneg => for a given volume fraction of electrolyte
c
c     - determine the size of the cell components...
c
      xnpos = float(npos)
      aconv = anspcap/aspcap
      awtrat = aratio/aconv
      adodf = aratio
      hi = height - 2.0*tcan
c     - q0 is the loading density in C/cc.
      q0 = dpos * aspcap
c     calculate radii and weights
      pi = 3.1415927
c     - ignore the values for rpcc and height given in the input,
c       and test a series of positive current collector radii (rpcc)
      do 10 ii=4,26,4
         rpcc = float(ii)/100.0
         vpos = tamphr*3600.0/q0/xnpos
         hi = vpos/pi/(2.0*rpcc*tpos + tpos**2)
         height = hi + 2.0*tcan
      vpcc = pi * (rpcc**2) * hi
      wpcc = vpcc * dpcc
      rpos = rpcc + tpos
      vtemp = pi * (rpos**2) * hi
      vpos = vtemp - vpcc
      wpos = vpos * dpos
      rsep = rpos + tsep
      vtemp = pi * (rsep**2) * hi
      vsep = vtemp - vpos - vpcc
      wsep = vsep * dsep
      rncc = rsep + tncc
      vtemp = pi * (rncc**2) * hi
      vncc = vtemp - vsep - vpos - vpcc
      wncc = vncc * dncc
      if (iamode .eq. 1) then
         wneg = wpos * awtrat * xnpos
         vneg = wneg/dneg
         rneg = sqrt((vneg + xnpos*(vncc+vsep+vpos+vpcc))/pi/hi)
         rcan = rneg + tcan
      else
         rneg = rcan - tcan
         wneg = (pi*(rneg**2)*hi - vtemp*xnpos) * dneg
         vneg = wneg/dneg
      endif
      wcan = (pi*hi*(rcan**2 - rneg**2) + 2.0*pi*(rcan**2)*tcan)*dcan
c     - electrolyte calculation is specific to the cell
c     - welec includes the weight of the separator
      delec = 1.6477
      welec=(vpos*xnpos*0.51 + vneg*0.25 + 0.8*vsep*xnpos)*delec/xnpos
```

```
      basewt=(wneg+wcan+feedwt)/xnpos + wpcc + wpos + welec + wncc
      amphr = q0 * vpos/3600.0
      tamphr = amphr * xnpos
      awtrat = wneg/wpos/xnpos
      aratio = awtrat*aconv
      adodf = aratio
      print 140,mode,iamode,vcut,aspcap,anspcap,ndata
 140  format(1x,/,1x,'mode = ',i2,5x,'iamode = ',i3,
     &       /,1x,'vcut = ',f12.5,' volts',
     &       /,1x,'aspcap = ',f17.6,5x,'anspcap = ',f17.6,' C/g',
     &       /,1x,'ndata = ',i5)
      print 141,height,rat1,rat2,npos,sepeff,y0,u0,q0,timed,feedwt
 141  format(1x,'height = ',f12.5,'cm',5x,'rat1 = ',f8.4,5x,
     &         'rat2 = ',f8.4,
     &       /,1x,'npos = ',i4,7x,'sepeff = ',f10.4,
     &       /,1x,'y0 = ',f12.5,5x,'u0 = ',f12.5,5x,'q0 = ',f12.5,
     &       /,1x,'timed = ',f12.2,'sec',5x,'feedwt =',f17.4,'grams',//)
      print *,'     TABLE OF COMPONENTS '
      print 150
 150  format(1x,'component',t20,'radius',t41,'thickness',t65,'density',
     & t89,'weight',t109,'conductivity')
      print 151,rpcc,dpcc,wpcc,spcc
 151  format(4x,'pcc',t13,f17.4,t59,f17.4,t82,f17.4,t105,f17.2
     & )
      print 152,rpos,tpos,dpos,wpos
 152  format(4x,'pos',t13,f17.4,t36,f17.4,t59,f17.4,t82,f17.4)
      print 153,rsep,tsep,dsep,wsep
 153  format(4x,'sep',t13,f17.4,t36,f17.4,t59,f17.4,t82,f17.4)
      print 154,rncc,tncc,dncc,wncc
 154  format(4x,'ncc',t13,f17.4,t36,f17.4,t59,f17.4,t82,f17.4)
      print 161
 161  format(1x,'---------')
      print 155,rneg,dneg,wneg
 155  format(4x,'neg',t13,f17.4,t59,f17.4,t82,f17.4)
      print 156,rcan,tcan,dcan,wcan
 156  format(4x,'can',t13,f17.4,t36,f17.4,t59,f17.4,t82,f17.4)
      print 157,rneg,dbus,sbus
 157  format(4x,'bus',t13,f17.4,t59,f17.4,t105,f17.2)
      print 158,dpost,spost
 158  format(3x,'post',t59,f17.4,t105,f17.2,//)
      print 160,welec,basewt,amphr,tamphr,aconv,awtrat,aratio
 160  format(1x,'welec = ',f17.4,5x,'basewt = ',f17.4,
     &       /,1x,'amphr = ',f17.4,5x,'tamphr = ',f17.4,
     &       /,1x,'aconv = ',f12.5,5x,'awtrat = ',f12.5,5x,'aratio = ',
     &            f12.5)
c
c     - begin calculations...
c
      call collector
      S1(1)=0.0
      S2(1)=0.0
```

```
      E2=0.0
      E4=0.0
      DO 2 I=2,NDATA
      DOD=1.0-QFRACT(I)
      DODD=(OPEN(I)-OPEN(I-1))/(QFRACT(I-1)-QFRACT(I))
      DRDD=(RESIST(I)-RESIST(I-1))/(QFRACT(I-1)-QFRACT(I))
      CUR=DOD/TIMED*vpos*q0
      V=OPEN(I)-RESIST(I)*CUR
      E3=E4
      E4=OPEN(I)-VCUT-RESIST(I)*CUR
      S1(I)=S1(I-1)+(OPEN(I)+OPEN(I-1))/2.*(QFRACT(I-1)-QFRACT(I))
      S2(I)=S2(I-1)+(RESIST(I)+RESIST(I-1))/2.*(QFRACT(I-1)-QFRACT(I))
      IF(E4.GT.0.0) GO TO 2
      F2=-E4/(E3-E4)
      GO TO 8
    2 continue
    8 SUM1=S1(I)+F2*(S1(I-1)-S1(I))
      SUM2=S2(I)+F2*(S2(I-1)-S2(I))
      OP=OPEN(I)+F2*(OPEN(I-1)-OPEN(I))
      RES=RESIST(I)+F2*(RESIST(I-1)-RESIST(I))
      DOD=1.-QFRACT(I)-F2*(QFRACT(I-1)-QFRACT(I))
      HALF=1.0-DOD/2.
      eight = 1.0 - dod*0.8
      cur = dod/timed*vpos*q0
      weight = basewt/1000.0
      DO 3 K=2,NDATA
    3 IF(QFRACT(K).LT.HALF) GO TO 4
      K=NDATA
    4 L=K
      F=(HALF-QFRACT(L-1))/(QFRACT(L)-QFRACT(L-1))
      RHALF= 1.0/(1.0/RESIST(L-1)+F*(1.0/RESIST(L)-1.0/RESIST(L-1)))
      OHALF=OPEN(L-1)+F*(OPEN(L)-OPEN(L-1))
      DO 5 K=2,NDATA
    5 IF(QFRACT(K).LT.eight) GO TO 6
      K=NDATA
    6 LE=K
      fe=(eight-QFRACT(le-1))/(QFRACT(le)-QFRACT(le-1))
      reight=1.0/(1.0/RESIST(le-1)+fe*(1.0/RESIST(le)-1.0/RESIST(le-1)))
      oeight=OPEN(le-1)+fe*(OPEN(le)-OPEN(le-1))
    9 PNOW=OP**2/4.0/(RES)/WEIGHT
      P0=OPEN(1)**2/4.0/(RESIST(1))/WEIGHT
      PHALF=OHALF**2/4.0/(RHALF)/WEIGHT
      peight = oeight**2/4.0/reight/weight
      VV=OP-CUR*RES
      ENERGY= vpos*q0/ WEIGHT*(SUM1-CUR*SUM2)/3600.0
      print *, ' '
      if (dod .gt. adodf) then
         print *,'AAM:****************************** error 200'
      endif
      print 106
      PRINT 102, DOD,CUR,RES,ENERGY,P0,PHALF,peight,PNOW,WEIGHT,VV,RCUT
```

```
  102 FORMAT (X,F6.4,F11.4,F10.7,7F10.4,F10.7)
  106 FORMAT (9HODEPTH OF,2X,7HCURRENT,3X,6HRESIST,4X,6HENER
     1GY,8X,20HSPECIFIC POWER, W/KG,17X,6HWEIGHT/ X,9HDISCHARGE, 4X,1HA,
     28X,3HOHM, 5X,7HW-HR/KG,5X,4HZERO
     &          ,6X,4HHALF,4x,6heighty,6X,3HEND, 6X,6
     3HKG/POS)
      print *,'*******************************************************'
 10   continue
      stop
      end
c*************************************************************************
c*    Subroutine COLLECTOR uses equation (4-8) to calculate the       *
c*    electrochemical and grid resistances associated with one        *
c*    electrode (RESIST).                                             *
c*************************************************************************
      SUBROUTINE collector
  101 FORMAT(1X,25HX IS BEYOND INTERPOLATION,3X,3HX= ,F6.4)
      DIMENSION RESIST(100),YI(100)
      COMMON /collect/NDATA,rpcc,rsep,rpos,tsep,spcc,hi,RESIST,YI
      common/andy/awtrat,aratio
      common/test/xpasr,xnasr
      pi = 3.14159265359
      JFLAG=0
      DO 1 I=1,NDATA
      CALL OY (Y,I,JFLAG)
      YI(I)=Y
         sqalpha = (rpcc**2)*spcc*alog(rsep/rpcc)/2.0/(rsep-rpcc)/y
         alpha = sqrt(sqalpha)
         xtanh = tanh(hi/alpha)
         resist(i) = alpha/pi/(rpcc**2)/spcc/xtanh
    1 IF (JFLAG.EQ.1) return
      RETURN
      END
c*************************************************************************
c*    Subroutine OY calculates the apparent open-circuit potential    *
c*    and the area specific conductance of the active material in     *
c*    the cell.                                                       *
c*************************************************************************
      SUBROUTINE OY (Y,I,JFLAG)
      DIMENSION QFRACT(100),OPEN(100)
      COMMON/OY/QFRACT,QMAX,OPEN,VCUT
      COMMON/collect/NDATA
      common/andy/awtrat,aratio
      common/test/xpasr,xnasr
      QFRACT(I)=1.-(FLOAT(I-1)/FLOAT(NDATA-1))
      xpdod = (1.0 - qfract(i))*100.0
      xndod = xpdod/aratio
      call xpos(xpdod,xposu,xpasr)
      call xneg(xndod,xnegu,xnasr)
      y = 1.0/(xpasr+xnasr)
      open(i) = xposu - xnegu
```

```
      IF (OPEN(I).LT.VCUT) JFLAG=1
      RETURN
      END
c*************************************************************************
c*    Subroutine XPOS calculates the apparent open-circuit potential  *
c*    and the area specific resistance of the positive active         *
c*    material in the cell.                                           *
c*************************************************************************
      subroutine xpos(xpdod,xposu,xpasr)
c     - positive U and ASR values for Kaun's cell
c     - positive apparent open-circuit potential values ...
      if (xpdod .le. 47.0) then
         xposu = 1.7851747 - 0.023658622*xpdod
     &           + 0.0010556085*xpdod**2 - 0.16266578e-4*xpdod**3
      else
         qmax = 806.3
         q = xpdod/100.0*qmax
         xposu = 1.364 - 1.08e-4*q + 0.12498*alog(1.0-(q/qmax)**4)
      endif
c     - positive ASR values ...
      x = xpdod/100.0
      xpasr = 0.6*x**2 - 0.13583*x + 0.509468
      return
      end
c*************************************************************************
c*    Subroutine XNEG calculates the apparent open-circuit potential  *
c*    and the area specific resistance of the negative active         *
c*    material in the cell.                                           *
c*************************************************************************
      subroutine xneg(xndod,xnegu,xnasr)
      q = 806.3 * (xndod/100.0) * 1.301
      xnegu = 0.017 + 3.6e-5*q
      xnasr = 0.133 + 0.3042e-2 * xndod
      return
      end
```

Sample Input for Program CYLINDER

```
1  1 0                          mode   iamode  itest
0.7292      1.25                   aratio  vcut
3216.9   3126.0                 aspcap  anspcap
100                               ndata
19.5   2.515                     height, rcan
0.1000                            rpcc
0.4  0.2  0.0117  0.042    thicknesses
10.2  2.686  1.90905  7.86  1.036  7.86  10.2  7.86     densities
69000.0   69000.0   19000.0                          conductivities
1.86  1.65                             rat1,rat2
11                                     npos
0.19                                 sepeff
1.5565   1.7682                        y0, u0
14400.0                             timed
50.0                                  feedwt
250.0                              tamphr
```

List of Variables from Program CYLINDER

adodf	DOD at which the negative capacity is exhausted
aload	loading density of the positive (g/cm^3)
amphr	capacity of one positive electrode (A-hr)
anload	loading density of the negative (g/cm^3)
anspcap	specific capacity of negative active material (C/g)
aspcap	specific capacity of positive active material (C/g)
awtrat	ratio of weights of negative to positive active materials
basewt	fraction of battery weight, excluding the bus and post weights, associated with one positive electrode (kg)
cap	delivered capacity (A-hr)
cur	current (A)
dbus	density of bus material (g/cm^3)
dcan	density of can material (g/cm^3)
delec	density of electrolyte (g/cm^3)
dncc	density of negative current collector (g/cm^3)
dneg	density of negative active material (g/cm^3)
dod	fractional depth of discharge of the positive active material
dodd	derivative of the apparent open-circuit potential (open) with respect to dod
dpcc	density of positive current collector (g/cm^3)
dpos	density of positive active material (g/cm^3)
dpost	density of post material (g/cm^3)
drdd	derivative of resist with respect to dod

dsep	density of separater (g/cm^3)
feedwt	feedthrough weight (g)
height	height of cell container (cm)
hi	height of positive current collector rod (cm)
iamode	flag - see code
mode	flag - see code
ndata	number of integration intervals
npos	number of positive electrodes per cell
oeight	apparent open-circuit potential 80% through discharge (V)
ohalf	apparent open-circuit potential halfway through discharge (V)
op	apparent open-circuit potential at the end of discharge (V)
open	array of apparent open-circuit potentials (V)
p0	maximum specific power when DOD=0 (W/kg)
peight	maximum specific power at 80% of discharge (W/kg)
phalf	maximum specific power halfway through discharge (W/kg)
pnow	maximum specific power at end of discharge (W/kg)
q0	loading density of positive active material (C/cm^3)
qfract	array of fractional state of charge values
qmax	loading of positive electrode per unit of separator area (C/cm^2)
rcan	outer radius of cell can (cm)
rcut	resistance of bus and post combination at end of discharge (Ω)
res	sum of electrochemical and grid resistances at the end of discharge (Ω)

resist	array containing the sum of the electrochemical and grid resistances (Ω)
rhalf	sum of electrochemical and grid resistances halfway through discharge (Ω)
rncc	outer radius of negative current collector (cm)
rneg	outer radius of negative active material (cm)
rpcc	outer radius of positive current collector (cm)
rpos	outer radius of positive active material (cm)
rprime	bus and post resistance (Ω)
rsep	outer radius of separator (cm)
s1	integral of open-circuit potentials
s2	integral of resistances
sbus	conductivity of the bus material (Ω^{-1}-cm^{-1})
sepeff	separater resistance ($\Omega \cdot cm^2$)
spcc	conductivity of the positive current collector ($\Omega^{-1} \cdot cm^{-1}$)
spost	conductivity of the post material (Ω^{-1}-cm^{-1})
tamphr	total capacity of cell (A-hr)
tcan	thickness of the cell container (cm)
tncc	thickness of the negative current collector (cm)
timed	time of discharge (sec)
totcap	total delivered capacity desired when mode=2 (A-hr)
tpos	thickness of the positive electrode bed (cm)
tsep	thickness of the separator (cm)
u0	initial apparent open-circuit voltage (V)
V	closed-circuit voltage (V)

vcut	cutoff voltage (V)
vncc	volume of negative current collector (cm^3)
vneg	volume of negative active material (cm^3)
vpcc	volume of positive current collector (cm^3)
vpos	volume of positive active material (cm^3)
vsep	volume of separator (cm^3)
wbus	weight of the bus (g)
wcan	weight of the can (g)
weight	basewt plus associated bus and post weights (kg)
welec	weight of electrolyte associated with one positive electrode (g)
wncc	weight of the negative current collector (g)
wneg	weight of the negative active material (g)
wpcc	weight of the positive current collector (g)
wpos	weight of positive active material (g)
wpost	weight of the post (g)
wprime	weight of the bus and post combination (g)
wsep	weight of the separator (g)
xnasr	area specific resistance of the negative ($\Omega \cdot cm^2$)
xndod	discharged fraction of negative capacity
xnegu	apparent open-circuit potential of the negative (V)
xpasr	area specific resistance of the positive ($\Omega \cdot cm^2$)
xpdod	discharged fraction of positive capacity
xposu	apparent open-circuit potential of the positive (V)
y0	initial value of electrochemical conductance ($\Omega^{-1} \cdot cm^{-2}$)
yi	array of values of electrochemical conductance ($\Omega^{-1} \cdot cm^{-2}$)

Appendix C

$LiAl/FeS_x$ Reactions

The following reaction sequences were taken from Bernardi [2].

Electrochemical Reactions of the FeS Electrode

1. $26FeS + Li^+ + Cl^- + 6K^+ + 6e^- \longrightarrow LiK_6Fe_{24}S_{26}Cl + 2Fe$ (J-phase)
2. $J + 25Li^+ + 20e^- + \longrightarrow 13Li_2FeS_2 + 11Fe + 6K^+ + Cl^-$ (X-phase)
3. $2FeS + 2Li^+ + 2e^- \longrightarrow Li_2FeS_2 + Fe$
4. $Li_2FeS_2 + 2Li^+ + 2e^- + \longrightarrow 2Li_2S + Fe$
5. $J + 51Li^+ + 46e^- + \longrightarrow 26Li_2S + 24Fe + 6K^+ + Cl^-$

Electrochemical Reactions of the FeS_2 Electrode

1. $2FeS_2 + 3Li^+ + 3e^- \longrightarrow Li_3Fe_2S_4$
2. $Li_3Fe_2S_4 + 0.47Li^+ + 0.47e^- + \longrightarrow 1.58Li_{2.2}Fe_{0.8}S_2 + 0.84Fe_{0.875}S$
3. $Fe_{1-x}S$ and $Li_{2+x}Fe_{1-x}S_2$ produce Li_2FeS_2
4. $Li_2FeS_2 + 2Li^+ + 2e^- + \longrightarrow 2Li_2S + Fe$

Electrochemical Reaction in the LiAl Electrode

1. $Li_yAl \longrightarrow yLi^+ + Al + ye^-$ (where y=1.0, for example)

Appendix D

Model Parameters

This appendix contains four tables that show the values of certain parameters that were used in the computer models.

Model Parameters for LiAl/FeS Prismatic Cell

electrolyte	LiCl-KCl
separator material	BN felt
separator porosity	85%
separator length (cm)	0.16
positive current collector grid material	Fe
negative current collector grid material	1008 steel
bus material	Fe
post material	Fe
loading density of the positive (g/cm^3)	2.30
specific capacity of positive active material (C/g)	2195.1
loading density of the negative (g/cm^3)	1.1182
specific capacity of negative active material (C/g)	3126.0
feedthrough weight (g)	50
thickness of the positive electrode (cm)	0.35
time of discharge (hours)	4
cutoff voltage (V)	0.9

Model Parameters for LiAl/2-P FeS_2 Prismatic Cell

electrolyte	LiCl-LiBr-KBr
separator material	BN felt
separator porosity	80%
separator length (cm)	0.2
positive current collector grid material	Molybdenum
negative current collector grid material	1008 steel
bus material	Fe
post material	Fe
loading density of the positive (g/cm^3)	1.719
specific capacity of positive active material (C/g)	3216.9
loading density of the negative (g/cm^3)	1.035
specific capacity of negative active material (C/g)	3126.0
feedthrough weight (g)	50
thickness of the positive electrode (cm)	0.35
time of discharge (hours)	4
cutoff voltage (V)	0.9

Model Parameters for LiAl/U-P FeS_2 Prismatic Cell

electrolyte	LiCl-LiBr-KBr
separator material	BN felt
separator porosity	80%
separator length (cm)	0.2
positive current collector grid material	Molybdenum
negative current collector grid material	1008 steel
bus material	Fe
post material	Fe
loading density of the positive (g/cm^3)	2.686
specific capacity of positive active material (C/g)	3216.9
loading density of the negative (g/cm^3)	1.035
specific capacity of negative active material (C/g)	3126.0
feedthrough weight (g)	50
thickness of the positive electrode (cm)	0.35
time of discharge (hours)	4
cutoff voltage (V)	1.25

Model Parameters for LiAl/U-P FeS_2 Cylindrical Cell

electrolyte	LiCl-LiBr-KBr
specific capacity of negative active material (C/g)	3126.0
specific capacity of positive active material (C/g)	3216.9
negative to positive active materials weight ratio	0.7504
can material	1008 Steel
negative current collector material	1008 Steel
positive current collector material	Molybdenum
density of negative active material (g/cm^3)	1.036
density of positive active material (g/cm^3)	2.686
separator material	BN felt
porosity of separator	80%
thickness of the separator (cm)	0.2
feedthrough weight (g)	50
thickness of the cell container (cm)	0.042
thickness of the negative current collector (cm)	0.0117
time of discharge (hours)	4
thickness of the positive electrode bed (cm)	0.4
cutoff voltage (V)	1.25

Appendix E

Additional Model Results

The following results are intended to supplement those found in Table 1 of Chapter 3. All three cells delivered 30 Ah in four hours, and the positive-electrode thickness was 0.35 cm for each. The bus and post resistances and weights were ignored.

Simulation Results for LiAl/FeS Prismatic Cell

Number of positive electrodes	1
Neg./Pos. Capacity Ratio	1.2
electrode area (cm^2)	76.74
negative electrode thickness (cm)	0.628
positive current collector weight (g)	22.67
negative current collector weight (g)	52.55
weight of positive active material (g)	55.03
weight of negative active material (g)	46.37
weight of cell can (g)	114.27
feedthrough weight (g)	50
weight of electrolyte (g)	99.32
total weight (g)	440.3
specific power at full charge (W/kg)	196
specific power at half discharge (W/kg)	120

Simulation Results for LiAl/2-P FeS_2 Prismatic Cell

Number of positive electrodes	1
Neg./Pos. Capacity Ratio	1.1
electrode area (cm^2)	75.34
negative electrode thickness (cm)	0.675
positive current collector weight (g)	30.18
negative current collector weight (g)	53.87
weight of positive active material (g)	42.33
weight of negative active material (g)	43.56
weight of cell can (g)	118.15
feedthrough weight (g)	50
weight of electrolyte (g)	84.88
total weight (g)	423.0
specific power at full charge (W/kg)	390
specific power at half discharge (W/kg)	226

Simulation Results for LiAl/U-P FeS_2 Prismatic Cell

Number of positive electrodes	1
Neg./Pos. Capacity Ratio	0.7
electrode area (cm^2)	88.17
negative electrode thickness (cm)	0.672
positive current collector weight (g)	33.20
negative current collector weight (g)	60.28
weight of positive active material (g)	74.06
weight of negative active material (g)	53.35
weight of cell can (g)	130.33
feedthrough weight (g)	50
weight of electrolyte (g)	90.29
total weight (g)	491.9
specific power at full charge (W/kg)	380
specific power at half discharge (W/kg)	262

Appendix F

Experimental Techniques

The apparent open-circuit potential and the area specific resistance were introduced in Chapter 2. These quantities are used to characterize the electrochemical behavior of cells. The apparent open-circuit potential is measured 15 seconds after dc-current interruption. Trost described the technique [10]:

> When the total external current is interrupted, we can identify three transients: relaxation of the double-layer capacity, a local equalization of charge and concentration from front to back of the electrode, and a reduction of concentration gradients in the whole cell by diffusion across the separator. In the current-interruption technique, we wish to wait long enough for double-layer charging to relax. A characteristic time for this is L^2aC/κ. The apparent open-circuit potential will continue to rise as the other transients continue. We choose 15 seconds here so that we may more closely approximate the results that would be obtained with a 15-second power test.

In the double-layer-charging time constant, L is the length of the porous electrode (cm), a is the specific interfacial area (cm^{-1}), C is the differential double-layer capacity (f/cm^2), and κ is the effective conductivity of the solution (mho/cm). The way in which the battery's open-circuit potential approaches steady state is shown in Figure 20.

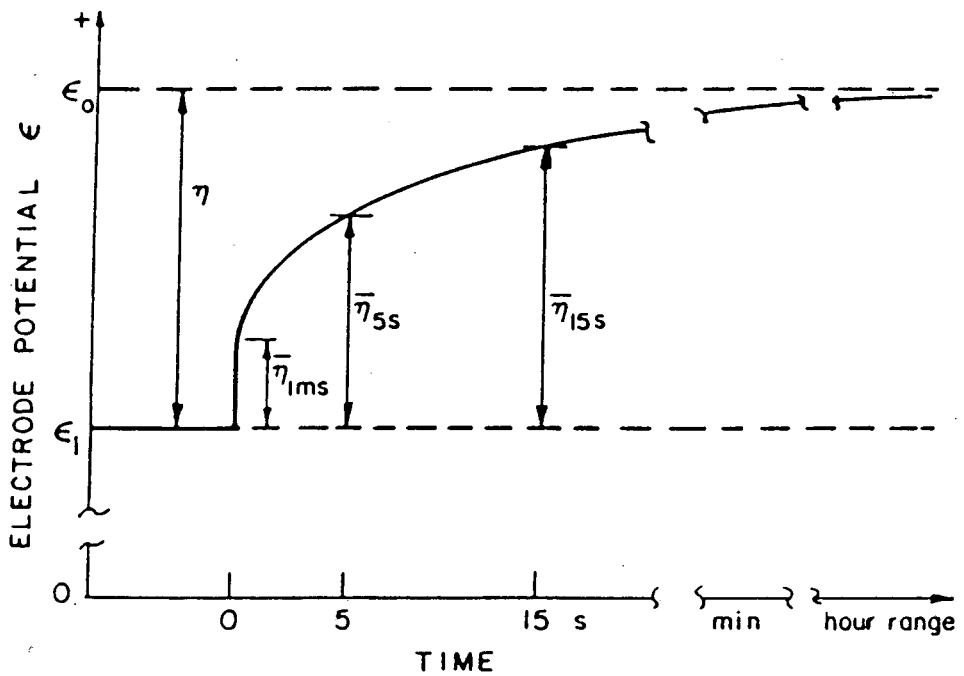

Figure 20. Potential relaxation after discharge current interruption. The ϵ_o is the open-circuit steady-state potential value, ϵ_i is the closed-circuit steady-state value, η is the electrode polarization as classically defined, $\bar{\eta}_t$ is the potential relaxation at time t; time zero indicates the instant of current interruption. Reproduced from reference 5, p. 136.

The use of reference electrodes is mentioned in Chapter 2. The apparent open-circuit potential of the positive electrode (U_+) is the voltage between the positive electrode's terminal and the reference electrode's lead. The data are referred to an α-β LiAl reference electrode, which was introduced by Argonne National Laboratory as a potential standard for testing of Li-alloy containing batteries [16]. The α-β LiAl electrode is based on the Fe/Li-Al (α and β phase)/Li^+ couple, and the emf of the electrode remains constant at about 300 mV relative to elemental lithium [17]. The reference electrode that was actually used to collect most of the data in Chapter 2 was based on the $Ni/Ni_3S_2/S^=$ couple. This electrode was found to possess the best long term stability for use as a reference electrode [17].

LAWRENCE BERKELEY LABORATORY
TECHNICAL INFORMATION DEPARTMENT
UNIVERSITY OF CALIFORNIA
BERKELEY, CALIFORNIA 94720